Thesis for the Degree of Master of Science

The Lattice Boltzmann Simulation on Wave Height Reducing Effect by Multi-structure under a Wave

The Graduate School

University of Ulsan

Department of Naval Architecture and Ocean Engineering

HAN YING

The Lattice Boltzmann Simulation on Wave Height Reducing Effect by Multi-structure under a Wave

Supervisor: Professor Rho-Taek Jung

A thesis

submitted to

the Graduate School of the University of Ulsan

In partial fulfillment of the requirements

for the Degree of Master

By

HAN YING

Department of Naval Architecture and Ocean Engineering

Ulsan, Korea

February 2020

The Lattice Boltzmann Simulation on Wave Height Reducing Effect by Multi-structure under a Wave

This certifies that the thesis of Han Ying is approved

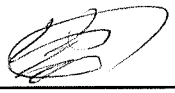

Committee Chair: Professor Yoon-Rak Choi

Committee Member: Professor Jin-Tae Lee

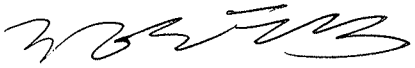

Committee Member: Professor Rho-Taek Jung

Department of Naval Architecture and Ocean Engineering

Ulsan. Korea

January 2020

Acknowledgements

During the master's study at Ulsan University, I was fortunate to be a disciple of the Professor Rho-Taek Jung. Thank you for giving me such a learning opportunity. Thank you also to the professor for the kindness, which made me feel warm in the intense learning atmosphere. In these two years of study, without his support and encouragement, I will not have the opportunity to improve my academic knowledge to another level.

I really thank to my thesis committee, Professor Yoon-Rak Choi and Professor Jin-Tae Lee for their helpful suggestions and opinions on my thesis.

At the same time, I would also like to thank all the professors of naval architecture and ocean engineering at Ulsan University for their wonderful lectures during my master study.

I would like to thank the senior. She patiently answered my doubts and explained the knowledge to me like a teacher before my thesis went smoothly.

I also want to thank my family for their support and encouragement behind them, so that I can study in peace in a foreign country.

There is a long way to go. Although the master's study process is over, the learning path is not over. I will carry on my original intentions and bring what I have learned into meaningful work.

Abstract

In the field of ship and ocean engineering, flow past body and wave motion are common hydrodynamic problems. In recent years, lattice Boltzmann method (LBM) has been developed to simulate fluid motion using particle system with specific evolution law. Firstly, in order to solve the problem of fluid structure coupling， the flow around a circular cylinder is studied based on the lattice Boltzmann method. The two-dimensional D2Q9 model, Single-Relaxation-Time Lattice Boltzmann Method, Multi- Relaxation-Time Lattice Boltzmann Method, the Smagorinsky eddy viscosity model under the large eddy simulation and impedance boundary conditions are used to simulate the flow. The boundary condition of Bouzidi surface is adopted for the solid surface, which makes the solid surface meet the condition of no slip. The flow around a cylinder with Reynolds numbers of 500, 1000 and 3900 is calculated. Compared with the Single- Relaxation-Time Lattice Boltzmann method, the Multi-Relaxation-Time simulation has the advantage of less instability in all simulations. The blocking ratio effect of flow around a cylinder in a channel is studied. The simulation results of predicting the force coefficient and vortex shedding frequency of MRT-LBM with different constant Smagorinsky model show that this method can improve the numerical stability of LBM in high Reynolds number simulation. On this basis, the second-order Stokes nonlinear wave generated by the mass source method is simulated by establishing a numerical simulation water tank. The VOF method is extended to the free surface tracking in the LB model, and the variation equation of the distribution function in each direction is applied to the mass source wave generation. The upper and outlet of the numerical simulation wave tank are set as open boundary, while the bottom is set as solid boundary. The movement of fluid through a single cylinder and a single square cylinder with free surface is simulated, and the variation of force and its coefficient is observed. In order to effectively reduce the wave height of free surface, three different types of multi-structures are installed in the domain. The same gap is set between the structure and the structure to simulate the change of wave height, and the force coefficient is analyzed. The numerical simulation results show that the numerical wave tank can effectively simulate the waves, avoid the secondary reflection of the waves in the calculation domain, have good wave elimination effect, and do not produce obvious reflected waves. It inherits the advantages of LB method, and has the characteristics of high calculation efficiency and internal parallel.

Keywords: MRT-LBM (Multi-Relaxation-Time Lattice Boltzmann Method), flow around a circular cylinder, multi-structure, wave breaker, mass source

List of Figures

Contents

Chapter 1

Introduction

With the continuous development of computational fluid dynamics, the paper published in the first lattice Boltzmann method (LBM) in 1988 has attracted the attention of many scholars. The Lattice Boltzmann method is derived from the improvement of the lattice gas automata (LGA) method of McNamara and Zanetti in 1988. It not only inherits the advantages of the lattice gas automata, but also overcomes some of the disadvantages of the lattice gas automata. Therefore, it is the inheritance and development of lattice gas automata. Different from the traditional CFD calculation method, the lattice Boltzmann method is based on the molecular motion theory, which is a discrete method in the macroscopic view and a continuous method in the microscopic sense, which is called a mesoscopic simulation method. Based on the theory of statistical mechanics, the "particle system" is constructed to calculate the motion and collision of particles, so as to obtain the macroscopic characteristics of the particles. Therefore, the fluid interaction description is simple, the complex boundary is easy to set, the calculation is easy, and the program is easy to implement. LBM has been widely recognized as an effective means of describing fluid motion and processing engineering problems. LBM is similar to microscopic method calculations, and is based on the fluid particle motion model of collision migration, which makes the handling of interactions inside the fluid easier. In the process of flow field evolution, the calculation process of each grid point is not affected by other grid points. The lattice Boltzmann method is characterized by the fact that the convection operator in the phase space is linear. A simplified particle distribution function is used instead of a hydrodynamic variable to simulate a simplified kinetic equation for fluid flow. Fluid is considered to be a combination of various fluid particles present on a lattice node. Each particle is associated with a particle distribution function in all possible directions. The interaction between particles is divided into two steps: collision and fluidization. The macroscopic density and velocity can be calculated from the microscopic particle distribution function. Based on the above characteristics, LBM makes it relatively intuitive to handle fluids and solids, and has obvious advantages in solving gas-solid and fluid-solid coupling. In 1991, Chen [1] proposed a single relaxation time method, using the same time relaxation coefficient to control the speed of different examples close to their respective equilibrium states, further simplifying the collision operator. Assuming that

density fluctuations are negligible, the incompressible Navier-Stokes equation can be recovered from the LB model by the Chapman-Enskog program (He et al., [2]). In order to improve the numerical stability of LBM, in recent years, LBM with multiple relaxation time mode has been developed and applied. The collision process of the multi-relaxation-time lattice Boltzmann method (MRT-LBM) is not carried out in the velocity space, but in the moment space. After the particle distribution function is projected into the poly space, the different moments correspond to density, momentum, energy and heat respectively. Different physical quantities such as flow and stress tensor can use different relaxation times for different moments in the collision process, thus increasing the flexibility of the model. The Lattice Boltzmann method is also useful for simulating complex boundary conditions and simulating single-phase and multi-phase fluids, and is easy to implement. The multi-relaxation time lattice Boltzmann model has been applied in the simulation of the flow in porous media [3], jet flow [4-6], cylinder flow [7], multi-phase flow [8] and so on. In real life, due to the large area of the ocean, most of the conditions are affected by turbulence. Therefore, in order to simulate turbulence with the lattice Boltzmann method, since the stability of the basic algorithm has its own limitations on the relaxation parameters, it needs to be extended. A better option is to combine the lattice Boltzmann method with the Smagorinsky model under the large eddy simulation (LES) model [9-10]. With the further development of computer technology and the gradual enrichment of computational methods, the lattice Boltzmann method will achieve more results and play an important role in the development of science and technology.

In the field of ship and ocean engineering, the floating of ocean platforms and the movement of torpedoes are inseparable from the study of fluid dynamics. With the advancement of science and technology, computational fluid dynamics, which was born through the combination of fluid dynamics theory and computer technology, has made fluid dynamics. Academic research is no longer limited to theoretical research and experimental analysis. The flow around is a classic hydrodynamic problem, and it is also a common physical phenomenon. The flow around a cylinder is a basic and complex flow, including the separation of flow, the generation and shedding of vortices, and the mutual interference of vortices. The study of flow around a cylinder not only has important basic theoretical significance but also has very important significance in engineering practice. For example, the role of water flow in bridges, offshore drilling platform pillars, offshore transport pipelines, pile foundation wharfs, etc., wind, tower equipment, chemical tower equipment,

high-altitude cables, etc., have important engineering application background. When the underwater structure is subjected to an outflow, it causes vortex-induced vibration of the structure, which causes damage to the structure after a long time. Therefore, in-depth study of the flow around the cylinder and analysis of its flow mechanism not only have theoretical significance, but also obvious social and economic benefits.

Due to the large sea area and the influence of external forces on the surface of the ocean, the free surface will produce various wave front conditions. When the various ship structures are working at sea, they will not only be affected by fluid turbulence, but also the free surface will also be Cause damage. Therefore, the simulation of wave making and wave elimination is extremely important for the field of ship and ocean engineering. However, in the actual application of the simulation, not only the investment is large, but also the investment time is large. In order to facilitate the simulation of wave making and wave elimination, the establishment of numerical wave tank for numerical simulation has become a research hotspot in the field of fluid mechanics. The mathematical model is the core part of the wave numerical simulation. Compared with traditional physical model tests, numerical water tanks have the advantages of low cost, no size limitation, easy modification, and accurate measurement. Wave trough numerical simulation is the basis for numerical simulation of port shoreline engineering. We can create waves of various shapes by adding a wave maker. In terms of wave making, most of the values are simulated with an extended computational domain, or the simulation is terminated when the fluctuations do not reach a quasi-steady state. In order to obtain long-term stable numerical simulation, the requirement of the numerical pool is to reduce the secondary reflected wave, and the target wave is not affected by the reflected wave. The wave method in the fluid domain can solve this problem well. Wave generators generally generate three different forms of linear waves, second-order Stokes nonlinear waves, and irregular waves. In terms of wave-eliminating, the traditional methods of clipping include the slope method and the sponge active absorbing method.

Based on the above description, this thesis first simulates the flow around the cylinder based on the single relaxation and multi-relaxation time lattice. At high Reynolds numbers, the multi-relaxation lattice Boltzmann method is combined with the Smagorinsky sub-grid model. In the wave making method, the mass source method is an effective method. Since the lattice Boltzmann method is a simple and effective fluid numerical simulation method, we derive the Bhatnagar-Gross-Krook (BGK) form of mass source method based on the lattice Boltzmann method to create a digital water tank. Pursue free surfaces by using the VOF

method for wave propagation. The feasibility of applying the LB model to numerical troughs is verified, and the effectiveness of the existing models is verified. The results show that the LBM-based quality source method can generate the required waveforms, which lays a foundation for subsequent research. It simulates the variation of wave height with time under the action of second-order waves and square columns. On this basis, in order to effectively reduce the wave-to-structure loss and maintain the wave-eliminating performance, three different forms of porous structures are inserted in the basin for the simulation of the wave-out, and the advantages and disadvantages of different forms of wave-eliminating are carried out. A comprehensive analysis, by comparing the wave height before and after the porous structure, gives the optimal settings.

Chapter 2

Background

All types of vessels navigating in the ocean (including all types of underwater vehicles navigating near the surface) and marine engineering structures operating in fixed seas are subject to waves. . When the sea is bad, the ship's pitch and heave will. The emergence of these problems has promoted the continuous development of ship hydrodynamics and the continuous improvement of the construction level of ships and marine engineering structures. Due to the water wave problem and the complexity of the interaction between wave and structure, many wave pools and wave sinks with different functions are constructed to carry out model test research under wave action. The motion situation is used to test theoretical calculations. In order to better solve the engineering problems such as the ship's sailing performance wave and structure interaction, it is necessary to constantly improve and improve the wave making and wave-eliminating technology of the wave pool. In series, through the deepening of theoretical exploration and the rapid development of computer technology, it is quite feasible to use numerical calculation to derive wave propagation and force analysis and motion analysis of structures in waves, called numerical waveguide technology.

2.1 Numerical Wave Maker

The numerical wave-making technique can be generally divided into three types: the first is the boundary element wave-making method based on the potential flow theory to restore the Laplace equation based on the potential flow theory; the second is based on solving the viscous incompressible fluid. The viscous numerical wave-making method of the NS equation; the third is the source function wave-making method which can be used as both a viscous fluid and an ideal fluid.

In the actual engineering practice, the ideal fluid does not exist, so the second method is suitable for solving the viscous numerical wave-making method of the NS equation of the viscous incompressible fluid. In the viscous numerical wave making, the most important thing is how to solve the shape and position of the free surface in real time. This should use a method called free surface tracking. There are many free surface tracking

methods, such as MAC method, VOF method and coordinate transformation method. Miyaca.H [11] uses the finite difference method to discretize the viscous fluid NS equation, combines the MAC method and the k-ε turbulence model to establish a two-dimensional numerical wave trough, and uses the velocity boundary wave-making method to generate short-period regular waves, which is very successful. The VOF method (ie, free surface tracking method) has been widely used due to its intuitiveness and scientific. The basic principle of the VOF method is to determine the free surface of the tracking fluid (the interface between two different fluids) by studying the fluid and mesh volume ratio function F in the grid unit, and to track the change of the fluid to achieve the free surface of the fluid. The VOF method is used to pursue the free surface. This method is simple and effective, and has good calculation results in practical engineering. For the source function wave-making method, in 1987, Brorsen and Larsen adopted the method of simulating "water blasting", and proposed the boundary element (BEM)-based mass source function wave-making method [12], which successfully simulated the two-dimensional linear rule wave. Nonlinear waves such as second-order Stokes waves. Since then, many scholars have begun to pay attention to the source wave making method and apply it to the N-S equation based on viscous fluids, and proposed a similar momentum source wave making method. 1999, Lin et al. [13] applied the mass source method effectively to the numerical wave trough based on the Navier-Stokes equation. 2017, Wang Kai and Yu Yang [14] combined the mass source method with the lattice Bozeman to successfully simulate the regular waves and second-order Stokes waves. In the process of numerical wave making, the regular wave is easier, but the numerical simulation of the irregular wave is relatively difficult, and it is very difficult to make the wave in the case of shaking or shaking on the surface of the water flow. If the LBM is combined with the mass source wave method and the VOF method is used to pursue the free surface, the wave numerical construction of the case is greatly helpful of vessels navigating in the ocean (including all types of underwater vehicles navigating near the surface) and marine engineering structures operating in fixed seas are subject to waves. When the sea is bad, the ship's pitch and heave will. The emergence of these problems has promoted the continuous development of ship hydrodynamics and the continuous improvement of the construction level of ships and marine engineering structures. Due to the water wave problem and the complexity of the interaction between wave and structure, many wave pools and wave sinks with different functions are constructed to carry out model test research under wave action. The motion situation is used to test theoretical calculations. In order to better

solve the engineering problems such as the ship's sailing performance wave and structure interaction, it is necessary to constantly improve and improve the wave making

2.2 Waver Breaker

In terms of numerical wave clipping, the most commonly used wave-splitting technique in the numerical wave pool is the Damping zone. The Damping Wavelet Zone is also known as the Digital Beach or Sponge Absorbing Layer. In other words, the principle is to simulate the sand absorbing method of the beach and the sponge to add artificial viscous terms on the boundary conditions of the specific self-exit surface to achieve the purpose of damping wave elimination. In 1981, aker et al. [15] introduced the concept of damping zone for the first time in its two-dimensional boundary element mode, which has since been widely adopted. He is characterized by the simultaneous addition of dissipative terms on the moving boundary conditions and dynamic boundary conditions of the free surface to dampen changes in the water level and potential function.

In addition, it is worth mentioning that the active wave generating-absorbing boundary is consciously applied to the wave machine to generate an "active" response while generating an incident wave. The reflected wave produced. Troch [16] established an active absorption wave-making theory suitable for multi-directional irregular waves. Using digital filtering technology, the wave front or wave velocity recording at a certain point in the water tank near the wave-making plate is entered, and the reflection wave is separated and adjusted. The wave-making signal causes the incident wave to absorb the reflected wave generated by the model, but only when the frequency of the incident wave coincides with the sampling frequency of the filter, a better absorption effect can be obtained. At the same time, due to the linear wave-making theory and linear control system, the calculation error increases with the increase of wave nonlinearity.

Chapter 3

Lattice Boltzmann Method

3.1 Lattice Boltzmann Method

The lattice Boltzmann method originated from the theory of gas dynamics. As we know, LGA has many advantages, but as a new kind of fluid model and calculation method, LGA also has some disadvantages, such as: statistical noise, exponential complexity of collision operator, not meeting Galileo invariance, etc. Lattice Boltzmann method is developed to overcome these shortcomings of LGA. In the lattice Boltzmann method, the particle distribution function is used instead of the particle itself in LGA to evolve. The lattice Boltzmann equation is directly used in the evolution equation, and the density and velocity of the fluid are calculated directly according to the distribution function. It describes how the particle distribution of the fluid changes with time, so the statistical noise is eliminated. At the same time, in the lattice Boltzmann model, the Boltzmann distribution is used instead of Fermi-Dirac distribution to satisfy the Galileo invariance.

3.1.1 Single-Relaxation-Time Lattice Bhatnagar-Gross-Krook model (SRT-BGK)

For system without an external force, the Boltzmann equation can be written as,

$$\frac{\partial f}{\partial t} + \mathbf{c}.\nabla f = \Omega \tag{3.1}$$

Here f represents the single particle distribution function and can be written as $f(\mathbf{r}, \mathbf{c}, t)$ where it means that the probability of finding a fictitious fluid particle in the lattice space $\mathbf{r}$ at a time t and with a certain velocity $\mathbf{c}$. The change in particle density in a specific position is due to the collision between particles and right hand side of the above equation is the collision operator. In 1954, Bhatnagar, Gross and Krook proposed the collision operator termed, BGK approximation [17].

$$\Omega = \omega(f^{eq} - f) = \frac{1}{\tau}(f^{eq} - f) \tag{3.2}$$

where $\omega = 1/\tau$. The coefficient ω is called the collision frequency and τ is called relaxation factor. The local equilibrium distribution function is denoted by f^{eq}, which is Maxwell–Boltzmann distribution function. The lattice Boltzmann evolution equation for Single-Relaxation-Time BGK model becomes,

$$\frac{\partial f}{\partial t} + \mathbf{c}.\nabla f = \frac{1}{\tau}(f^{eq} - f) \tag{3.3}$$

Applying an explicit finite different scheme to the above equation, the complete discretized form is [9],

$$f_i(\mathbf{x} + \mathbf{e}_i\Delta t, t + \Delta t) - f_i(\mathbf{x}, t) = -\frac{1}{\tau}[f_i(\mathbf{x}, t) - f_i^{eq}(\mathbf{x}, t)] \tag{3.4}$$

Streaming Collision

where $\mathbf{e}_i$ is a discrete velocity vector and Δt is the advancing time step. So the left side of equation is streaming step in which each particles moves to nearest node in the direction of its velocity. The right side is 'collision' step which occurs when particles arriving at a node interact and change their velocity directions according to scattering rules. Fig 3.1 shows how the streaming step and collision step take place for the interior nodes.

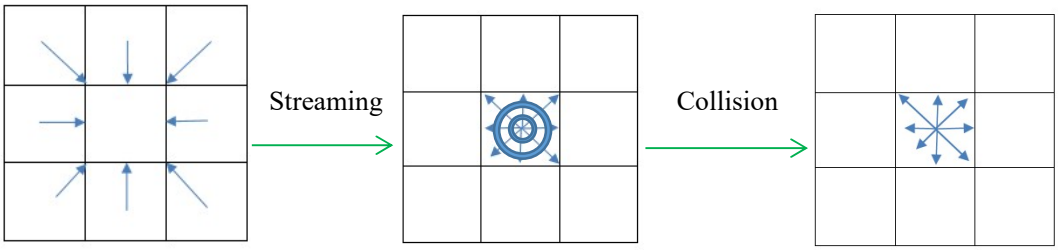

Figure 3.1 Streaming and Collision of D2Q9 model.

LBM models can be found in all three dimensions. The nomenclature used to refer the different possible arrangements is D*d*Q*q*, where *d* says how many dimensions and *q* for possible directions of velocity vectors. In one-dimension, there are D1Q3 and D1Q5 models. For two-dimension D2Q4, D2Q5, D2Q7 and D2Q9 can be found. D3Q15 or D3Q19 or D3Q27 model is used for three-dimensional simulation. In this thesis, two dimensional D2Q9 model as in Fig 3.2, is utilized for all simulations.

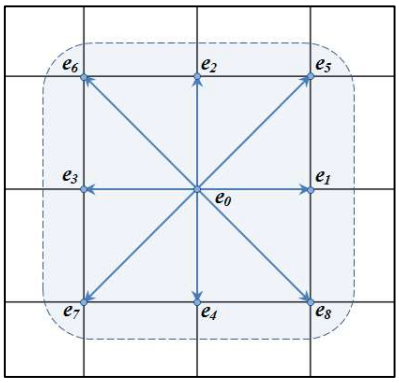

Figure 3.2 The discrete velocities for D2Q9 model.

For a two-dimensional flow, a particle is restricted to stream in a possible of 9 directions with nine discrete velocities. One zero rest velocity in the center, four velocities pointing towards the neighboring cells in horizontal and vertical direction and another four velocities towards the diagonal neighbors. The particle velocities are therefore defined as:

$$\mathbf{e}_i = \begin{cases} (0,0), & i = 0 \\ \left(\cos\left[\frac{(i-1)\pi}{2}\right], \sin\left[\frac{(i-1)\pi}{2}\right]\right)c, & i = 1 \sim 4 \\ \left(\cos\left[\frac{(2i-9)\pi}{4}\right], \sin\left[\frac{(2i-9)\pi}{4}\right]\right)\sqrt{2}c, & i = 5 \sim 8 \end{cases} \tag{3.5}$$

where $c = \frac{\Delta x}{\Delta t}$ is the lattice speed with Δt and Δx being the discrete time step and lattice spacing respectively.

The macroscopic density ρ of the fluid can be defined as a summation of microscopic particle distribution function,

$$\rho = \sum_{i=0}^{8} f_i \tag{3.6}$$

and the macroscopic velocity $\mathbf{u}$ which can be computed simply as an average of the microscopic velocities $\mathbf{e}_i$ weighted by the directional densities f_i, can be defined as

$$\rho\mathbf{u} = \sum_{i=0}^{8} \mathbf{e}_i f_i \tag{3.7}$$

The equilibrium distribution functions can be defined as

$$f_i^{eq}(\mathbf{x},t) = \rho w_i \left[1 + \frac{\mathbf{e}_i.\mathbf{u}}{c_s^{\,2}} + \frac{1}{2}\frac{(\mathbf{e}_i.\mathbf{u})^2}{c_s^{\,4}} - \frac{1}{2}\frac{\mathbf{u}^2}{c_s^{\,2}} \right] \tag{3.8}$$

The speed of sound in this model is $c_s = c/\sqrt{3}$ and w_i are weighting factors for different directions and defined as

$$w_i = \begin{cases} \frac{4}{9}, & i = 0 \\ \frac{1}{9}, & i = 1 \sim 4 \\ \frac{1}{36}, & i = 5 \sim 8 \end{cases} \tag{3.9}$$

and the equation of state is that of an ideal gas,

$$p = \rho c_s^2 = \frac{\rho}{3} \tag{3.10}$$

The relaxation time is related to the kinematics viscosity by

$$\upsilon = \frac{2\tau - 1}{6}\frac{(\Delta x)^2}{\Delta t} \tag{3.11}$$

In LBM approach, the lattice speed $c = \frac{\Delta x}{\Delta t}$ is mostly assumed as equal to 1. It means that Δx equals to 1 and Δt equals to 1. By changing time step Δt, it will result in changing of relaxation time τ because Δt is related to τ with the equation (3.11). Since relaxation time τ changes, the non-equilibrium parts of distribution functions also change with the equation (3.4). And also, the equilibrium parts of distribution functions change because the equilibrium part depends on the lattice speed c_s by equation (3.8). Therefore, the changing of time step will affect to changing of all distribution functions which in turn changes the flow characteristics; density and velocity.

3.1.2 Multi-Relaxation-Time Lattice Boltzmann Method (MRT LBM)

For simplicity, single-relaxation time BGK models are widely used. However, single-relaxation time model sometimes suffers from numerical instability and unsteadiness. Therefore, Multi-relaxation time (MRT) model was introduced by representing the collision operator in matrix form for better stability and steadiness (D. d'Humières [18]).

The evolution equation can be written as:

$$f_i(\mathrm{x}+\mathrm{e_i}\delta_\mathrm{t},\mathrm{t}+\delta_\mathrm{t})-\ f_i(\mathrm{x},\mathrm{t})=\ -\Omega\left[f_i(x,t)-f_i^{eq}(x,t)\right] \tag{3.12}$$

Where Ω is the collision matrix. In the velocity space, implementing of full matrix into the collision step is difficult. For that reason, the velocity space is transformed into moment space and the full collision matrix is transformed into a diagonal matrix, which leads to much convenience in performing the collision process. Therefore, the multi-relaxation-time lattice Boltzmann equation becomes

$$f(\mathrm{x}+\mathrm{e_i}\delta_\mathrm{t},\mathrm{t}+\delta_\mathrm{t})-\ f(\mathrm{x},\mathrm{t})=\ -\boldsymbol{M^{-1}S}\left[\boldsymbol{m}(x,t)-\boldsymbol{m^{eq}}(x,t)\right] \tag{3.13}$$

where $\boldsymbol{m}(x,t)$ and $\boldsymbol{m^{eq}}(x,t)$ are vectors of moments, $\boldsymbol{m}=(m_0,m_1,m_2,\dots m_n)^T$. And $\boldsymbol{S}$ is a diagonal matrix.

The linear transformation between the velocity space and moment space is done by the matrix M, which serves as a transformation matrix, and maps the distribution functions $\boldsymbol{f}(x,t)$ to their moments $\boldsymbol{m}(x,t)$.

$$\boldsymbol{m}=\boldsymbol{M}\,\boldsymbol{f} \tag{3.14}$$

$$\boldsymbol{f}=\ \boldsymbol{M^{-1}}\,\boldsymbol{m} \tag{3.15}$$

The transformation matrix M for D2Q9 model is given by

$$\mathbf{M}=\begin{bmatrix} 1 & 1 & 1 & 1 & 1 & 1 & 1 & 1 & 1\\ -4 & -1 & -1 & -1 & -1 & 2 & 2 & 2 & 2\\ 4 & -2 & -2 & -2 & -2 & 1 & 1 & 1 & 1\\ 0 & 1 & 0 & -1 & 0 & 1 & -1 & -1 & 1\\ 0 & -2 & 0 & 2 & 0 & 1 & -1 & -1 & 1\\ 0 & 0 & 1 & 0 & -1 & 1 & 1 & -1 & -1\\ 0 & 0 & -2 & 0 & 2 & 1 & 1 & -1 & -1\\ 0 & 1 & -1 & 1 & -1 & 0 & 0 & 0 & 0\\ 0 & 0 & 0 & 0 & 0 & 1 & -1 & 1 & -1 \end{bmatrix}$$

where a = 1/36.

The moment vector $\boldsymbol{m}$ is

$$\boldsymbol{m}=\left(\rho,e,\epsilon,j_x,q_x,j_y,q_y,p_{xx},p_{xy}\right)^T \tag{3.16}$$

Based on the equilibrium distribution function of an incompressible single-relaxation-time LBM model, the corresponding equilibrium moments, $\boldsymbol{m^{eq}}$ are obtained by

$$
\begin{aligned}
m_0^{eq} &= \rho \\
m_1^{eq} &= -2\rho + 3(j_x^2 + j_y^2) \\
m_2^{eq} &= \rho - 3(j_x^2 + j_y^2) \\
m_3^{eq} &= j_x \\
m_4^{eq} &= -j_x \\
m_5^{eq} &= j_y \\
m_6^{eq} &= -j_y \\
m_7^{eq} &= \left(j_x^2 - j_y^2\right) \\
m_8^{eq} &= j_x\, j_y
\end{aligned}
\tag{3.17}
$$

$$j_x = \rho u_x = \sum_i f_i^{eq} c_{ix} \;\; and \;\; j_y = \rho u_y = \sum_i f_i^{eq} c_{iy} \tag{3.18}$$

A diagonal matrix, $\boldsymbol{S}$ whose components represent the relaxation time of the moments, is

$$\boldsymbol{S} = diag(s_0, s_1, s_2, s_3, s_4, s_5, s_6, s_7, s_8) \tag{3.19}$$

where s_7 and s_8 are $1/\tau$, and s_3 and s_5 are arbitrary, can be set to 1.0.

The kinematic viscosity of the model can be calculated as

$$v = \frac{1}{3}\left(\frac{1}{s_8} - \frac{1}{2}\right) = \frac{1}{3}\left(\frac{1}{s_7} - \frac{1}{2}\right) \tag{3.20}$$

3.2 Smagorinsky sub-grid model

Smagorinsky (1963) suggested that, the idea of sub-grid model is based on an assumption to include the physical effects that the unresolved motion has on the resolved fluid motion. A formula for calculating the viscosity coefficient of sub-grid scales with time and space position is established. The hypothesis takes the turbulent stresses to be proportional to the mean rate of strain. The effect of the unresolved scales is modeled through an effective relaxation time scale τ_t. Thus the total LES effective relaxation time should be

$$\tau_{total} = \tau_t + \tau_0 \tag{3.21}$$

where $\tau_0$and τ_t are the relaxation times corresponding to the molecular viscosity $\upsilon_0$and the turbulence or eddy viscosity υ_0, respectively. τ_t depends on the sub-grid model used in the

simulation. In the LES, the most common sub-grid model is the Smagorinsky one. Using Smagorinsky model, the relaxation time in LBM is modified as follows. First, the non-equilibrium stress tensor $\Pi_{\alpha,\beta}$ is calculated for each cell with

$$\Pi_{\alpha,\beta} = \sum_{i=1}^{9} \mathbf{e}_{i\alpha}\mathbf{e}_{i\beta}\left(f_i - f_i^{eq}\right) \tag{3.22}$$

Thus, α and β each run over the two spatial dimensions, while i is the index of the respective velocity vector. The intensity of the local stress tensor S is then computed as

$$\mathrm{S}=\frac{1}{6\mathrm{C}^2}\left(\sqrt{\upsilon^2+18\mathrm{C}^2\sqrt{\Pi_{\alpha\beta}\,\Pi_{\alpha\beta}}}-\upsilon\right) \tag{3.23}$$

Now the modified relaxation time is given by

$$\tau_{total} = 3\left(\upsilon+\mathrm{C}^2\mathrm{S}\right)+\frac{1}{2} \tag{3.24}$$

It can be seen that S will always have a positive value thus the local viscosity will be increased depending on the size of the stress tensor calculated from the non-equilibrium parts of the distribution functions of the cell to be relaxed. This effectively removes instabilities due to small values of τ. Where C is the model experience coefficient and the value is 0.1.

3.3 Boundary Conditions for Lattice Boltzmann Method

The boundary conditions play an important role in the numerical simulation. In this thesis, the bounce-back or no-slip boundary condition is implemented at the bottom wall. The non-equilibrium bounce-back for pressure or velocity is applied at the inlet and outlet region. The Bouzidi's boundary condition for the curved geometry is also introduced here. And the multi-direct forcing immersed boundary condition coupled with lattice Boltzmann method is used for structure. Last but not least, the VOF-like single phase free surface boundary condition is employed to deal with the wave surface.

3.3.1 Bounce-back boundary condition

The half-way bounce-back scheme is used to obtain non-slip boundary conditions on the walls. Bounce-back scheme means that when a fluid particle distribution streams to a wall node, the particle distribution will scatter back to the fluid node with its incoming direction. For a node near a boundary, some of its neighboring nodes lie outside of the flow domain.

Therefore, the distribution functions at these nodes are undefined. The undefined distribution functions are shown in red color in Fig 3.3. The bounce-back scheme is a simple way to fix these unknown distributions on the wall node. Particles will arrive at the wall node from the fluid node. Particles arriving at the wall node bounce back and are sent back to the fluid node in the opposite direction of incoming particles (see Fig 3.3).

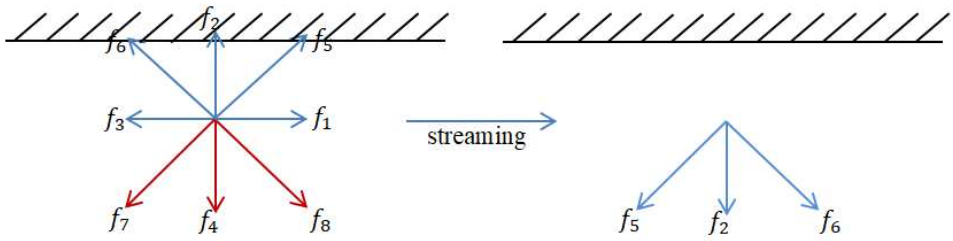

Figure 3.3 Illustration of bounce-back boundary condition

3.3.2 Non-equilibrium bounce-back boundary conditions

In 1997, Zou and He[19] studied the two-dimensional and three-dimensional LBGK models, and assumed that the non-equilibrium part of the distribution function still satisfies the bounce format in the direction perpendicular to the boundary, and then proposes a new boundary processing format, called non equilibrium bounce-back scheme. And is a way to specify pressure or velocity on flow boundaries, based on the idea of bounce-back of the non-equilibrium distribution. It is well known as Zou and He boundary condition and it can be used in the inlet and outlet boundary. Take an inlet boundary as an example. Suppose u and v are specified on the inlet. After streaming f_2, f_3, f_4, f_6, f_7 are known. The unknown distribution functions are shown in red color in Fig 3.4. We need to determine unknown functions f_1, f_5, f_8, ρ. By using equation (3.6) and (3.7), we get

$$f_1 + f_5 + f_8 = \rho - (f_0 + f_2 + f_3 + f_4 + f_6 + f_7) \tag{3.25}$$

$$f_1 + f_5 + f_8 = \rho u + f_3 + f_6 + f_7 \tag{3.26}$$

$$f_5 - f_8 = \rho v - f_2 + f_4 - f_6 + f_7 \tag{3.27}$$

By solving the above equations,

$$\rho = \frac{1}{1-u} - (f_0 + f_2 + f_4 + 2(f_3 + f_6 + f_7)) \tag{3.28}$$

Zou and He assume the bounce-back rule is still correct for the non-equilibrium part of the particle distribution normal to the boundary.

$$f_1 - f_1^{eq} = f_3 - f_3^{eq} \tag{3.29}$$

With the known value of f_3, we get

$$f_1 = f_3 + \frac{2}{3}\rho u \tag{3.30}$$

$$f_5 = \frac{1}{2}\rho v + \frac{1}{6}\rho u - \frac{1}{2}(f_2 - f_4) + f_7 \tag{3.31}$$

$$f_8 = \frac{1}{6}\rho u - \frac{1}{2}\rho v + \frac{1}{2}(f_2 - f_4) + f_6 \tag{3.32}$$

The similar procedure can be applied to the outlet too. For the outlet, pressure is supposed to be specified. After streaming f_1, f_2, f_4, f_5, f_8 are known (see Fig 3.4). We need to determine f_3, f_6, f_7, u. By using equation (3.6) and (3.7), we get

$$f_3 + f_6 + f_7 = \rho - (f_0 + f_1 + f_2 + f_4 + f_5 + f_8) \tag{3.33}$$

$$f_3 + f_6 + f_7 = -\rho u + f_1 + f_5 + f_8 \tag{3.34}$$

$$f_6 - f_7 = \rho v - f_2 + f_4 - f_5 + f_8 \tag{3.35}$$

By solving the above equations,

$$u = \frac{(f_0 + f_2 + f_4 + 2(f_1 + f_5 + f_8))}{\rho} - 1 \tag{3.36}$$

Assume the bounce-back rule is still correct for the non-equilibrium part of the particle distribution normal to the boundary.

$$f_1 - f_1^{eq} = f_3 - f_3^{eq} \tag{3.37}$$

With the known value of f_1, we get

$$f_3 = f_1 - \frac{2}{3}\rho u \tag{3.38}$$

$$f_6 = \frac{1}{2}\rho v - \frac{1}{6}\rho u - \frac{1}{2}(f_2 - f_4) + f_8 \tag{3.39}$$

$$f_7 = -\frac{1}{6}\rho u - \frac{1}{2}\rho v + \frac{1}{2}(f_2 - f_4) + f_5 \tag{3.40}$$

The corner node at the boundary needs a special treatment. For example, take a bottom inlet node at the intersection of two boundaries. After streaming, f_3, f_4, f_7 are known (see Fig 3.4).

ρ is assumed as the same ρ of its neighboring fluid node. u and v are zero at the corner node. Using bounce-back for the normal distributions gives

$$f_1 = f_3 \, , f_2 = f_4 \tag{3.41}$$

By using equation (3.6) and (3.7),

$$f_5 - f_6 + f_8 = -(f_1 - f_3 - f_7) = f_7 \tag{3.42}$$

$$f_5 + f_6 - f_8 = -(f_2 - f_4 - f_7) = f_7 \tag{3.43}$$

And then

$$f_5 = f_7 \tag{3.44}$$

$$f_6 = f_8 = \frac{1}{2}\,[\rho - (f_0 + f_1 + f_2 + f_3 + f_4 + f_5 + f_7)] \tag{3.45}$$

The other 3 corner nodes at the boundary can apply the similar procedure as above.

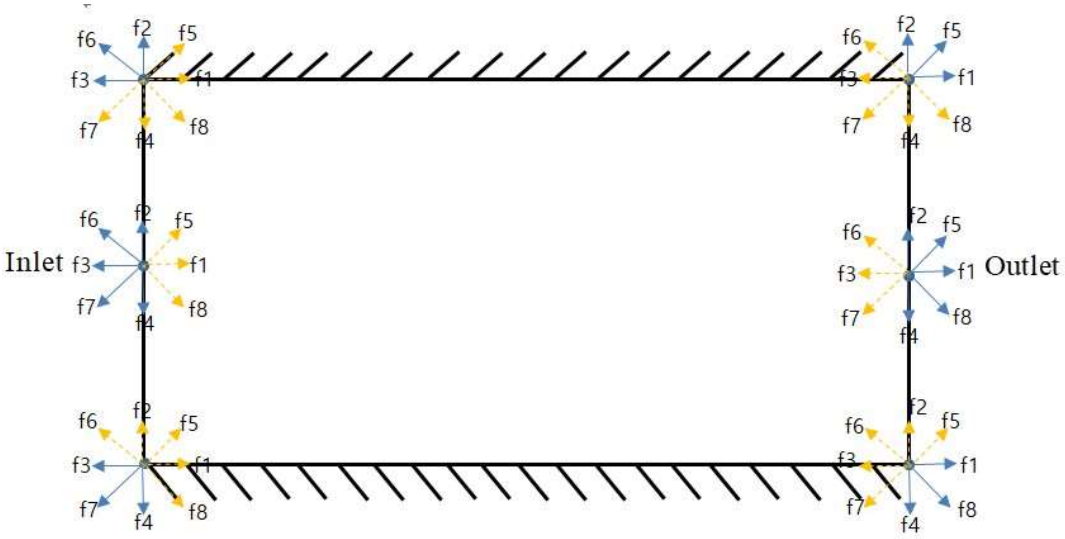

Figure 3.4 Schematic plots of velocity directions at inlet and outlet.

3.3.3 Bouzidi's boundary condition

A simple way to deal with boundaries of arbitrary geometry in the LBE method is proposed by Bouzidi by combination of the ‘‘bounce-back’’ scheme and spatial interpolations of first or second order [20].

Fluid nodes are on the left with A being the last one near the wall. B is the first solid node to the right of the wall. The location of the wall is given by $q = |AC|/|AB|$. See Fig 3.5. After the collision step, the distribution function of particles at fluid node coming back from the wall is not known. To calculate unknown distribution functions, the following scheme is proposed.

The scheme is considered in two cases according to the value of q, the distance between fluid node and wall. In both cases we use linear or quadratic interpolation formulas involving values at two or three nodes.

Suppose $\mathbf{r}_l$ is a fluid node such that $\mathbf{r}_l + \mathbf{c}_i$ is a solid node. Call $\mathbf{c}_{i'}$ the reversed velocity of $\mathbf{c}_i$ ($\mathbf{c}_{i'} = -\mathbf{c}_i$). By using linear interpolation

$$\begin{aligned} &\text{if } q < \frac{1}{2}, \qquad f_{i'}(\mathbf{r}_l, t+1) = 2q f_i^c(\mathbf{r}_l, t) + (1-2q) f_i^c(\mathbf{r}_l - \mathbf{c}_i, t) \\ &\text{if } q \geq \frac{1}{2}, \qquad f_{i'}(\mathbf{r}_l, t+1) = \frac{1}{2q} f_i^c(\mathbf{r}_l, t) + \frac{(2q-1)}{2q} f_{i'}^c(\mathbf{r}_l, t) \end{aligned} \tag{3.46}$$

By using quadratic interpolation

$$\begin{aligned} &\text{if } q < \frac{1}{2}, \qquad f_{i'}(\mathbf{r}_l, t+1) = q(2q+1) f_i^c(\mathbf{r}_l, t) + (1+2q)(1-2q) f_i^c(\mathbf{r}_l - \mathbf{c}_i, t) \\ &\qquad\qquad - q(1-2q) f_i^c(\mathbf{r}_l - 2\mathbf{c}_i, t) \\ &\text{if } q \geq \frac{1}{2}, \qquad f_{i'}(\mathbf{r}_l, t+1) = \frac{1}{q(2q+1)} f_i^c(\mathbf{r}_l, t) + \frac{(2q-1)}{2q} f_{i'}^c(\mathbf{r}_l, t) \\ &\qquad\qquad + \frac{(1-2q)}{(1+2q)} f_{i'}^c(\mathbf{r}_l - 2\mathbf{c}_i, t) \end{aligned} \tag{3.47}$$

On the right hand-side of Equation (3.46) and (3.47), the f^c are taken after collision and before propagation. The $f(., t+1)$ on the left-hand side will be used at values after collision and after propagation, that is after a complete LBE time step.

This Bouzidi scheme is used in calculating the unknown distribution functions around the circular cylinder in this thesis.

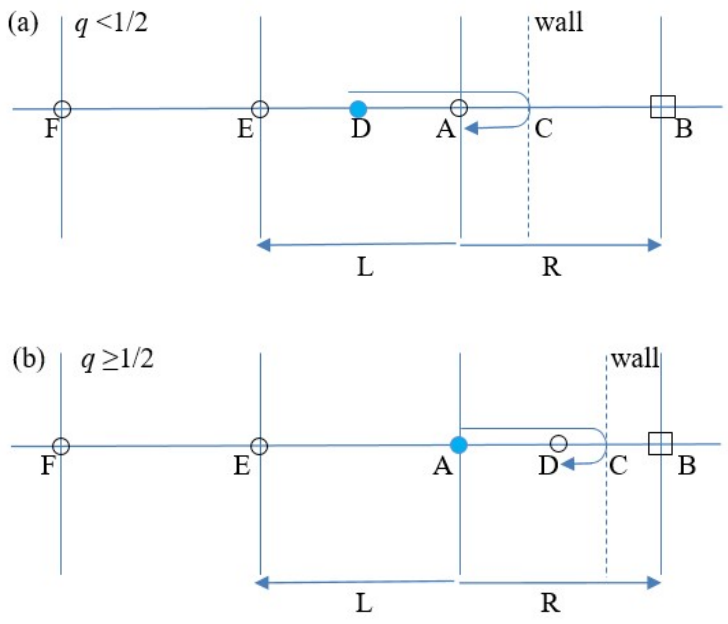

Figure 3.5 Details of the collision process for velocities of opposite direction

3.3.4 Tracking of Interface Movement and Free surface boundary

The movement of the free surface is computed directly from the distribution functions. The interface is tracked by the calculation of the mass that is contained in each cell. This requires two additional values to be stored for each cell: the mass m, and the fluid fraction ϵ. The fluid fraction is computed with the cell mass and density [21]

$$\epsilon = m/\rho \tag{3.48}$$

Where ϵ is the fluid fraction of cell. The volume fraction ϵ of fluid is 1 and that of gas is 0. All cells are allowed to change their state. It is important to note that direct phase change from fluid to gas or vice versa is not permitted. Hence, fluid or gas cells are only allowed to transform into interface cells whereas interface cells can be transformed into either gas or fluid cells. The interface cells that separate the gas phase and fluid phase are shown in Fig 3.6. [22]

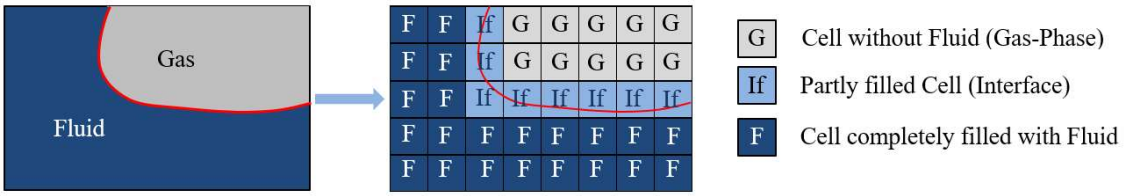

Figure3.6 Types of cell required for the free surface treatment.

During the streaming, the interface advection is done by the mass exchange between interface cell and fluid cell or between two interface cells. For an interface cell and a fluid cell at $(\mathbf{x}+\Delta t\mathbf{e}_i)$ this is given by:

$$\Delta m_i(\mathbf{x},t+\Delta t)=f_{\bar{i}}(\mathbf{x}+\Delta t\mathbf{e}_i,t)-f_i(\mathbf{x},t) \tag{3.49}$$

The first part of right side is the amount of fluid entering the cell at current time step, the second one is leaving the cell. The area of fluid interface has to be taken into account the mass exchange for two interface cells. It is approximated by averaging the fluid fraction values of two cells. Which becomes,

$$\Delta m_i(\mathbf{x},t+\Delta t)=s_e\frac{\epsilon(\mathbf{x}+\Delta t\mathbf{e}_i,t)+\epsilon(\mathbf{x},t)}{2} \tag{3.50}$$

With $s_e=f_{\bar{i}}(\mathbf{x}+\Delta t\mathbf{e}_i,t)-f_i(\mathbf{x},t)$. It holds the fact that fluid leaving one cell has to enter other one $\Delta m_i(\mathbf{x})=-\Delta m_i(\mathbf{x}+\Delta t\mathbf{e}_i)$. For interface cells with fluid neighbor, the mass change has to conform to the distribution functions exchanged during streaming, as fluid cells don't need additional computations. Their fluid fraction is one and mass is the current density. After adding the mass change values for all directions for interface cells, resulting in the mass for the next time step;

$$m(\mathbf{x},t+\Delta t)=m(\mathbf{x},t)+\sum_{i=0}^{8}\Delta m_i(\mathbf{x},t+\Delta t) \tag{3.51}$$

Since gas phase, in this thesis, is regarded as air and no distribution function is directly advected from gas to fluid cell or interface cell. So that at the free surface, the reconstruction of distribution functions from the empty cell is needed. Moreover, it is assumed that the viscosity of the fluid is significantly lower than that of the gas phase, while having a higher density. Hence, the gas follows the fluid motion at the interface. In terms of distribution functions, this means that if at $(\mathbf{x}+\Delta t\mathbf{e}_i)$ there is an empty cell:

$$f_i^{'}(\mathbf{x},t+\Delta t)=f_i^{eq}(\rho_A,\mathbf{u})+f_{\bar{i}}^{eq}(\rho_A,\mathbf{u})-f_i(\mathbf{x},t) \tag{3.52}$$

The pressure of the atmosphere onto the fluid interaction is introduced by using ρ_A for the density of the equilibrium distribution functions. An atmospheric pressure of $\rho_A = 1$ is used, as this is also the reference density and pressure of the fluid. Applying equation to all directions with empty neighbor cells would result in a full set of distribution functions for interface cells. While empty and fluid cells have a mass of exactly zero and one, interface cells that have filled or emptied usually have an excess mass on conversion. This excess mass that can be positive or negative needs to be distributed to the neighboring interface cells. In order to do this, the mass is not just distributed evenly among the surrounding interface cells, but weighted according to the direction of the interface normal **n**.

$$m(\mathbf{x}+\Delta t\mathbf{e}_i)=m(\mathbf{x}+\Delta t\mathbf{e}_i)+m^{ex}(\eta_i/\eta_{total}) \tag{3.53}$$

Here η_{total} is the sum of all weights η_i , each of which is computed as

$$\eta_i=\begin{cases}\mathbf{n}\cdot\mathbf{e}_i & if \quad \mathbf{n}\cdot\mathbf{e}_i>0\\ 0 & otherwise\end{cases} \qquad for \quad filled \quad cells, and \tag{3.54}$$

$$\eta_i=\begin{cases}-\mathbf{n}\cdot\mathbf{e}_i & if \quad \mathbf{n}\cdot\mathbf{e}_i<0\\ 0 & otherwise\end{cases} \qquad for \quad emptied \quad cells \tag{3.55}$$

During simulation, there is the situation that the single interface cells are left behind when the fluid moves on, or interface cells get enclosed in fluid. To alleviate that artifacts, these cells are needed to be forced either empty or filled depends on their flags.

3.3.5 An extrapolation method for boundary conditions

Continuing with the concept of the interpolation scheme, Guo et al. [23] introduce an extrapolation method for boundary condition.

The particle distribution functions are composed of equilibrium and non-equilibrium parts. The non-equilibrium part can be approximated by extrapolating from the neighboring fluid nodes. The equilibrium part can be determined by a fictitious equilibrium distribution where the boundary conditions is enforced.

The unknown incoming post collision distribution functions can be defined as

$$f_i(\rho,u)=f_i^{eq}(\rho,u)+(1-\tfrac{1}{\tau})f_i^{neq}(\rho,u) \tag{3.56}$$

where the unknown ρ and u can be extrapolated from the interior nodes. With the extrapolated values of ρ and u, the equilibrium distribution functions can be calculated by

$$f_i^{eq} = \rho_w + \rho_0\left(\frac{e_i \boldsymbol{u}}{c_s^2} + \frac{(e_i.\boldsymbol{u})^2}{2c_s^4} - \frac{\boldsymbol{u}^2}{2c_s^2}\right) \tag{3.57}$$

The non-equilibrium part can be approximated by the non-equilibrium part of the distribution function at the fluid node with second order accuracy.

3.3.6 Non-reflecting pressure boundary condition

To reduce the reflected waves at the outlet boundary, Finck et al. [24] proposed a relaxation procedure as follow. The pressure P_b at the exit boundary x_b is assumed to be relaxing to its final prescribed value P_{out} in the following form:

$$\frac{\partial}{\partial t}(P_b - \rho c_s u_n) + \alpha(P_b - P_{out}) = 0 \tag{3.58}$$

where,

u_n = the flow velocity normal to the boundary

c_s = thermal speed of sound

α = constant parameter

The above equation can be discretized in an explicit manner for a new time level by

$$P_b^n = \frac{P_b^{n-1} + \rho c_s(u_n - u_n^{n-1}) + \alpha \Delta t P_{out}}{1 + \alpha \Delta t} \tag{3.59}$$

The unknown normal velocity u_n can be extrapolated from inside fluid nodes. The resulting new pressure P_b^n is used in calculating the equilibrium function equation (3.57) at the boundary.

3.4 Force evaluation

3.4.1 Momentum Exchange Method

In present study, the conventional momentum exchange method will be adopted and integrated in the lattice Boltzmann equation to evaluate forces exerted on the wedge surface. The momentum of the fluid in a cell is represented by eq. (3.7). In fact, the momentum expressed in the latter equation can be regarded as a vectors superposition summation of the

eight momentum components. In the streaming step, the distribution function $\widetilde{f_\alpha}$ will migrate from a site x to its neighbor lattice at site $\boldsymbol{x} + \boldsymbol{e_\alpha}$, the momentum component $\boldsymbol{e_\alpha f_\alpha}$ will transfer from the original lattice to the target lattice as well. The distribution functions bounced back from the solid surface are computed by eq. (3.46) and eq.(3.47), in which the boundary positions between the solid and fluid nodes are known and well treated. Considering the consistency, the bounced-back distribution functions and their respective momenta can be interpreted as a streaming out of the solid nodes. In this present method, the momentum exchange between the fluid and the solid particle is obtained on the point that links fluid and solid.

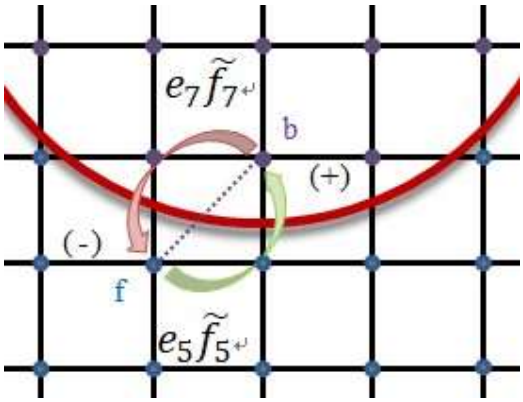

Figure 3.7 Fluid-Solid momentum-exchange**.**

The momentum $e_{\tilde{\alpha}}\widetilde{f}_\alpha$ goes into the solid particle and contributes a momentum increment to it. For the reverse direction, $e_{\tilde{\alpha}}\widetilde{f}_\alpha$ goes out of the solid particle and contributes a momentum decrement to it (Fig. 3.8).

So, the momentum-exchange value on the fluid-solid link, namely the force, can be written as (Mei and Shyy [25]); Li and Fang [26]):

$$F = \sum_{all\ x_b} \sum_{\alpha \neq 0} e_{\tilde{\alpha}} \left[\widetilde{f}_\alpha(x_b, t) + \widetilde{f}_{\tilde{\alpha}}(x_b + e_{\tilde{\alpha}}\delta t, t) \right] \times [\, 1 - w(x_b + e_{\tilde{\alpha}})]$$

Where $\mathbf{w}(\mathbf{x_b} + \mathbf{e}_{\tilde{\alpha}})$ is an indicator, who liiiiich is 0 at fluid node and 1 at solid boundary, $\mathbf{x_b}$. For a non-zero lattice velocity$\mathbf{e_\alpha}$, $\mathbf{e}_{\tilde{\alpha}}$ denotes the velocity in opposite direction. The inner summation calculates the momentum exchange between a solid node at $\mathbf{x_b}$ and all possible neighboring fluid nodes around that solid node over a time step. The outer summation calculates the force contribution over all boundary nodes $\mathbf{x_b}$ belonging to the body.

Chapter 4
Flow past a circular cylinder

Flow past a circular cylinder is one of the most widely used problems for Computational Fluid Dynamic (CFD) Flow past a circular cylinder has a simple geometry but it reveals a range of complex fluid phenomena, such as boundary layer separation and vortex shedding. This phenomenon plays an important role in ocean engineering problems because a detailed understanding of this flow essential element of designing behavior is the hydrodynamic structures. This flow past a circular cylinder at low Reynolds number by using LBM has been simulated by several researchers. However, the flow at high Reynolds number is still a challenging problem. Unlike lid-driven cavity flow, the flow past a circular cylinder has an obstacle in the flow. The handling of boundary condition at the inlet and outlet plays an important role in the simulation.

4.1 Computational set up

For the simulation of flow past a circular cylinder, a computation size of domain 1280 x 256 lattice unit is used. A geometry sketch is shown in Fig. 4.1. The present problem has a circular cylinder with diameter D. The blockage ratio, B = H/D =5 is used. The channel length, L is fixed at L/D = 25. An upstream length, l = 10D has been chosen. On top and bottom walls, we use non-slip bounce-back boundary condition. At the inlet of the computational domain, boundary condition proposed by Zou and He is used with given inlet velocity [19]. Impedance boundary condition has been used at the outlet boundary [27]. On the surface of the cylinder, we use boundary condition proposed by Bouzidi et al. [20].

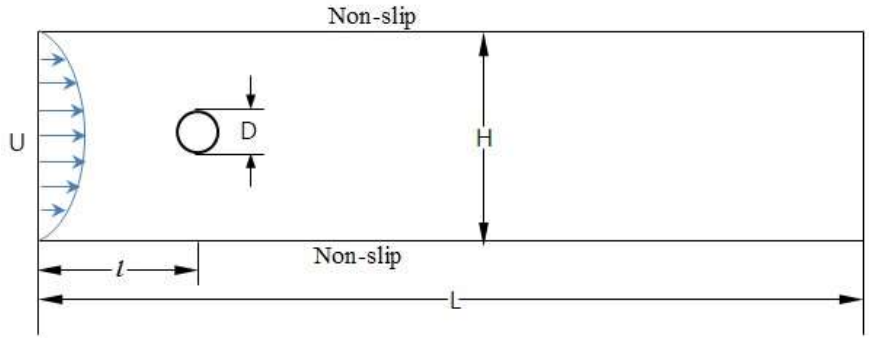

Figure 4.1 A geometry sketch of the flow past a circular cylinder confined in a channel.

4.2 SRT and MRT comparison

In this Section, we perform a comparison between SRT and MRT flow simulations. SRT and MRT simulations are performed under the same parameters and boundary condition as mentioned before. Fig. 4.2 compares vorticity contour of SRT and MRT simulations. There are jiggles around cylinder in SRT simulation and it becomes more serious when the Reynolds number goes high. In contrast, it cannot be found that kind of instability in MRT simulations. It is clearly pointed out that MRT gives more stable results than SRT at higher Reynolds number flow. When Reynolds number is higher, the relaxation parameter becomes closer to 0.5. LBM has its limit that can simulate until relaxation time is 0.5. It can enhance the instability occurred by the fact of relaxation time close to 0.5 by using multiple relaxation time.

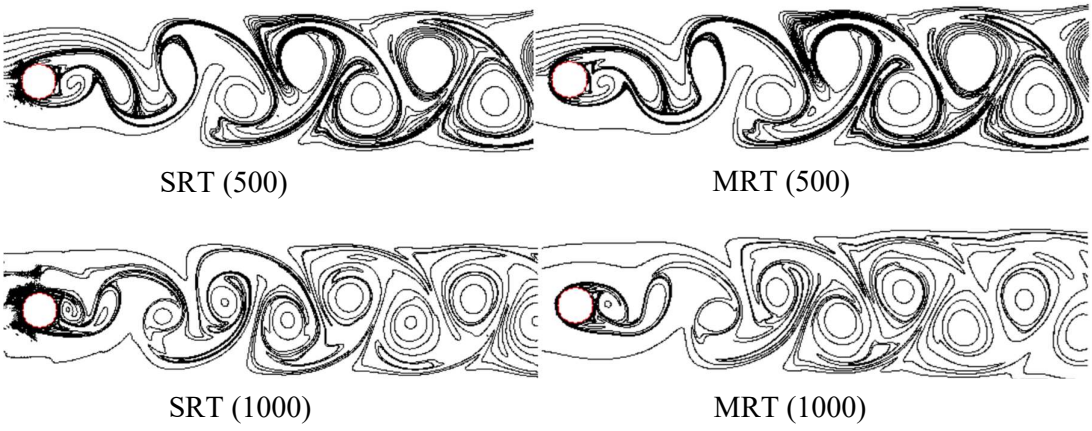

Figure 4.2 Vorticity contour of flow past a circular cylinder by using SRT and MRT at Re 500 and Re 1,000.

4.3 Blockage ratio effect on flow parameters

In this section, blockage ratio effect on flow parameter is examined numerically at Reynolds number 1,000 by using MRT LBM with Smagorinsky model. When the flow around a body is examined experimentally, the flow field is practically unbounded in most cases, whereas in a numerical solution, external boundaries are imposed, whose distance from the body depends on the extent of the computational domain. It is expressed as the blockage ratio, B = H/D. Four different blockage ratios such as B=5, B=8, B=10 and B=20 were used for the investigation of the blockage effect.

By having the total force acting on the cylinder, the drag coefficient and lift coefficient can be calculated as:

$$C_D = \frac{F_x}{\frac{1}{2}\rho U_\alpha^2 D}, \quad C_L = \frac{F_y}{\frac{1}{2}\rho U_\alpha^2 D} \tag{4.1}$$

where U_α is the free-stream velocity and D is the cylinder diameter. Strouhal number which is used to study the frequency of cylinder can be calculated by $S_t = \frac{fD}{U_\alpha}$ where f is the natural vortex shedding frequency.

The calculated drag coefficient, lift coefficient and Strouhal number of vortex shedding at different blockage ratio are shown in Fig. 4.3. Drag coefficient and lift coefficient decrease as the blockage ratio increases. The drag coefficient decreases 12.23%, lift coefficient decreases 8.19% and Strouhal number decreases 8.18% when blockage ratio increases from B=5 to B=8. There is only 1.74% decrease in drag coefficient, 1.07% decrease in lift coefficient and 0.41% increase in Strouhal number from B=10 to B=20. Therefore, blockage ratio B=10 is chosen for the reduction of computational time required. For further cases of the flow past a circular cylinder in this study, B=10 is used to simulate.

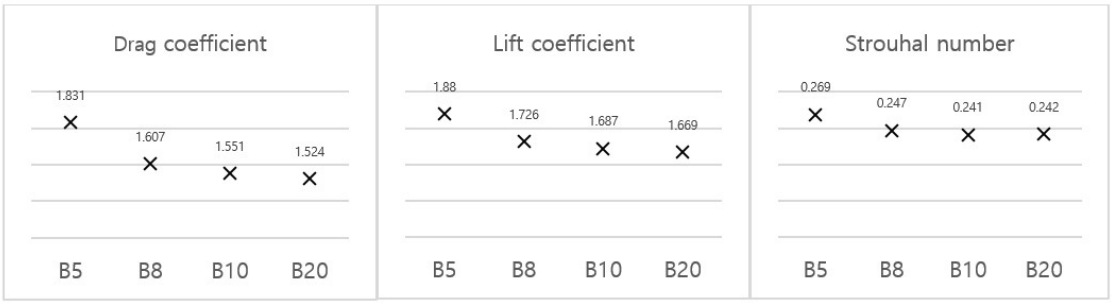

Figure 4.3 Effect of blockage ratio on flow parameters of flow past a circular cylinder at Re=1,000 (B refers to blockage ratio) considerably different from those of an unbounded solution.

Blockage ratio effects are significant for the accuracy of the results of a numerical solution. As a result of using low blockage ratio for the reduction of computational time, the values of various hydrodynamic parameters may be considerably different from those of an unbounded solution.

4.4 Results for the flow past a circular cylinder by using MRT LBM with Smagorinsky model

Streamline patterns, the contour plot for pressure and vorticity of the flow past a circular cylinder at Re=1,000 and Re=3,900 are shown in the Figure 4.4. The drag coefficient and Strouhal number comparing with other literature results are summarized in Figure 4.5. The present calculated results show well agreement with the literature data.

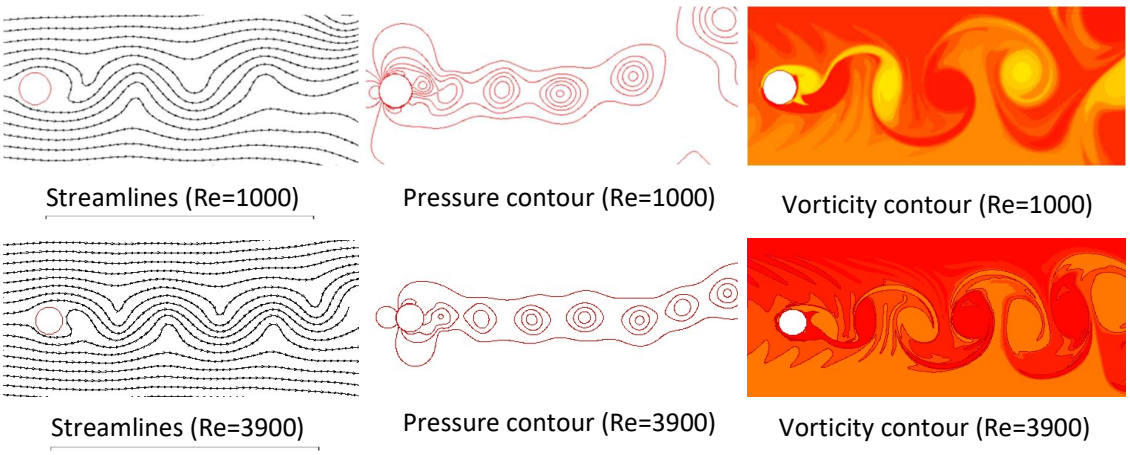

Figure 4.4 Streamline patterns, pressure contours and vorticity contours of flow past a circular cylinder at Reynolds numbers 1,000 and 3,900.

	Cd	St
Present work	1.683	0.259
Chen et al. [28]	1.827	0.255
Beaudan and moin [29]	1.740	0.263
Kravchenko and Moin [30]	1.650	0.230

Figure 4.5 Comparison of flow parameter at Re 3,900 with literature data.

Finally, the flow is simulated at various Smagorinsky constant 0.15, 0.1, 0.05 and 0.03 to study the effect of Smagorinsky constant on the flow. As C_S is related to relaxation time according to equation (3.24), the smaller C_S gives low viscous flow. As a result, it shows that a higher drag and lift coefficient at the smaller C_S value. At Reynolds number 3,900, Smagorinsky constant greater than 0.03 should be used to simulate the flow because using

small C_S 0.03 causes lower relaxation time. It means that eddy viscosity is not sufficient to damp the high-frequency fluctuations.

Chapter 5
Wave makers and Wave generation

Since ships are closely related to the ocean, the study of sea conditions is the basis of ship operation. However, due to the large ocean area and complex sea conditions, the actual observation of sea conditions requires a lot of funds and space. Therefore, we set up numerical simulation water tanks to conduct sea state research. For free surface problems, several LBE methods have been developed. Among these methods, a method similar to LBE VOF is adopted in this thesis, and the free surface is regarded as a single-phase flow. Therefore, the air portion is not touched and is considered a gas or an empty cell. The free surface motion is tracked by calculating the mass flux between the units, and the change in mass is calculated directly from the LBE distribution function. In order to generate the required waves, researchers have developed different wave generators placed in numerical tanks, such as piston-type, flap-type wave makers, cylindrical wave makers, plunger wave makers or snake wave makers. In this study, we will focus on the mass source wave method. Based on the introduction of the first chapter and the second one, we have learned that the internal mass source function based on the Naiver-Stokes equation developed by Lin et al. Wave making works through the function of an internal mass source. By introducing an external force term into the governing equation, it is possible to generate waves from the internal mass source function in the entrance region. Can generate various wave trains, including the linear monochromatic wave, irregular wave, stokes wave, solitary wave and cnoidal wave. In this study, second-order stokes wave is simulated and compared with analytical solutions.

5.1 Wave generation by internal mass source function

In the presence of a body force density and a mass source, the LBE must be modified to account for the force by adding an additional term to the LBE [31].

$$f_i(\mathbf{x}+\mathbf{e_i}\Delta t, t+\Delta t) - f_i(\mathbf{x},t) = -\frac{1}{\tau}[f_i(\mathbf{x},t) - f_i^{eq}(\mathbf{x},t)] + \Delta t\mathbf{F}_i \tag{5.1}$$

The equilibrium distribution function is:

$$f_i^{eq}(\mathbf{x},t) = f_i^{eq}(\rho^*, \mathbf{u}^*) \tag{5.2}$$

With the macro parameter

$$\rho^* \mathbf{u}^* = \sum_{i=0}^{\circ} \mathbf{e}_i f_i + m_2 \mathbf{F} \Delta t, \tag{5.3}$$

$$\rho^* = \sum_{i=0}^{\circ} f_i + m_1 S \Delta t, \tag{5.4}$$

Where S is the mass source and **F** is the body force, m_1 and m_2 are constant. After the detailed calculation to recover the final Navier-Stokes equation (with a mass source) [14, 31],

$$\frac{\partial \rho}{\partial t} + \nabla(\rho \mathbf{u}) = S \tag{5.5}$$

$$\frac{\partial \rho \mathbf{u}}{\partial t} + \nabla(\rho \mathbf{u}\mathbf{u}) = -\nabla p + \upsilon \nabla\left[\rho\left(\nabla \mathbf{u} + (\nabla \mathbf{u})^T\right)\right] + \mathbf{F} \tag{5.6}$$

$\mathbf{F}_i$ becomes,

$$\mathbf{F}_i = \left(1 - \frac{1}{2\tau}\right) w_i \left\{\left[\frac{\mathbf{e_i} - \mathbf{u}}{c_s^2} + \frac{\mathbf{e_i} \cdot \mathbf{u}}{c_s^4}\mathbf{e_i}\right]\mathbf{F} + \left[\frac{\mathbf{e_i}\mathbf{e_i}}{2c_s^2} + 2\right] S\right\} \tag{5.7}$$

To generate a desired wave through an internal mechanism, there are several options. One option is to introduce a mass source function in the continuity equation inside the computational domain. Theoretically, this mass source could be a point source, a line source, or a finite volume source. Another option is to apply an additional forcing function in the momentum equation (5.6). In this thesis, line source is employed in the inlet region. So that the conservation of mass can be modified as follows [31].

$$\nabla \mathbf{u} = s(x, y, t) \quad in \quad \Omega \tag{5.8}$$

where $(x, y, t) = S/\rho$, mass source within the source region Ω. Since the total mass of waves generated must be equal to the mass added by source function, the relation becomes

$$\int_0^t \int_{\Omega} s(x, y, t) d\Omega dt = \int_0^t \int_0^h \mathbf{u}(x, y, t) dh dt = \int_0^t C\eta(x, t) dt \tag{5.9}$$

where $\mathbf{u}(x, y, t)$ is the horizontal particle velocity and C is the phase velocity of the desired wave. For shallow water approximation, $C = \sqrt{g(h + y)}$, for deep water, $C = gT/2\pi$ and for intermediate water depth, $C = \sqrt{gtanh(kh)/k}$, respectively . For the position at (x , y) at time t within the mass source region,

$$s(x,y,t)\Delta x\Delta y\Delta t = \mathbf{u}(x,y,t)\Delta y\Delta t$$

then, $$s(x,y,t) = \frac{\mathbf{u}(x,y,t)}{\Delta x} \tag{5.10}$$

For a linear monochromatic wave, the horizontal wave particle velocity is

$$\mathbf{u}(x,y,t) = \frac{H\omega}{2}\frac{\cosh(k(y+h))}{\sinh(kh)}\cos(kx-\omega t) \tag{5.11}$$

where H stands for wave height, h is the water depth, $\omega = 2\pi/T$ is wave frequency with period T and $k = 2\pi/L$ is wave number with wave length L . The mass source is

$$s(x,y,t) = H\omega\frac{\cosh(k(y+h))}{\sinh(kh)}\cos(kx-\omega t) \tag{5.12}$$

The surface wave profile is

$$\eta(x,t) = \frac{H}{2}\cos(kx-\omega t) \tag{5.13}$$

For second-order stokes wave, the equations of horizontal velocity and mass source are

$$\mathbf{u}(x,y,t) = \frac{H\omega}{2}\left[\frac{\cosh(k(y+h))}{\sinh(kh)}\cos(kx-\omega t) + \frac{3Hk}{8}\frac{\cosh(2k(y+h))}{\sinh^4(kh)}\cos 2(kx-\omega t)\right] \tag{5.14}$$

$$s(x,y,t) = H\omega\left[\frac{\cosh(k(y+h))}{\sinh(kh)}\cos(kx-\omega t) + \frac{3Hk}{8}\frac{\cosh(2k(y+h))}{\sinh^4(kh)}\cos 2(kx-\omega t)\right] \tag{5.15}$$

The wave surface profile is

$$\eta(x,t) = \frac{H}{2}\cos(kx-\omega t) - \frac{H^2k}{8\sinh 2kh} + \frac{H^2k}{16}\frac{\cosh(2k(y+h))}{\sinh^3(kh)}\cos 2(kx-\omega t) \tag{5.16}$$

For cnoidal wave, Wiegel showed that surface profile can be described by [32]

$$\eta(x,t) = y_t + Hcn^2\left[2K(m)\left(\frac{x}{L}-\frac{t}{T}\right), m\right] \tag{5.17}$$

Where y_t is the distance between the still water level and wave trough, cn is the Jacobian elliptic function associated with the cosine, and *K(m)* is the complete elliptic integral of the first kind with modulus *m*. The wavelength *L*, phase speed C and wave period T are related to H, h and m by;

$$L = h\sqrt{\frac{16}{3}\frac{mh}{H}}K(m) \tag{5.18}$$

$$C = \sqrt{gh}\left[1+\frac{H}{mh}\left(1-\frac{1}{2}m-\frac{3}{2}\frac{E(m)}{K(m)}\right)\right] \tag{5.19}$$

The source function is

$$s(x,y,t) = C\left\{y_t + Hcn^2\left[2K(m)\left(\frac{x}{L}-\frac{t}{T}\right),m\right]\right\} \tag{5.20}$$

For a Solitary wave,

$$\eta(x,t) = H\,\mathrm{sech}^2(K(x-Ct)) \tag{5.21}$$

where $K = \sqrt{3H/4h^3}$ and $C = \sqrt{gh}\left(1+\frac{H}{2h}\right)$, the source function becomes

$$s(x,y,t) = CH\,\mathrm{sech}^2(K(x-Ct)) \tag{5.22}$$

5.2 Numerical experiments

Firstly , we consider a two-dimension case of second order wave generations on a constant water depth. The wave height H=0.002 m, wave length λ=0.0604 m, in the water depth h=0.01m with the period T=0.22 s is generated. For intermediate water depth, kh is kept around 1.04, which is the same parameter as in Lin et al [13]. Gravity is set as $g = 9.8\ m/s^2$ and water viscosity is $\upsilon = 1 \times 10^{-6}\ m^2/s$. The computational domain is $0.30\ m \times 0.016\ m$ and grid size is set as $2000 \times 80 (x \times y)$. The linear source is located at the left side of the computational domain. Non-slip boundary condition is applied at the bottom and left boundaries. Open boundary condition is implemented at the right side of domain (see figure 5.1).

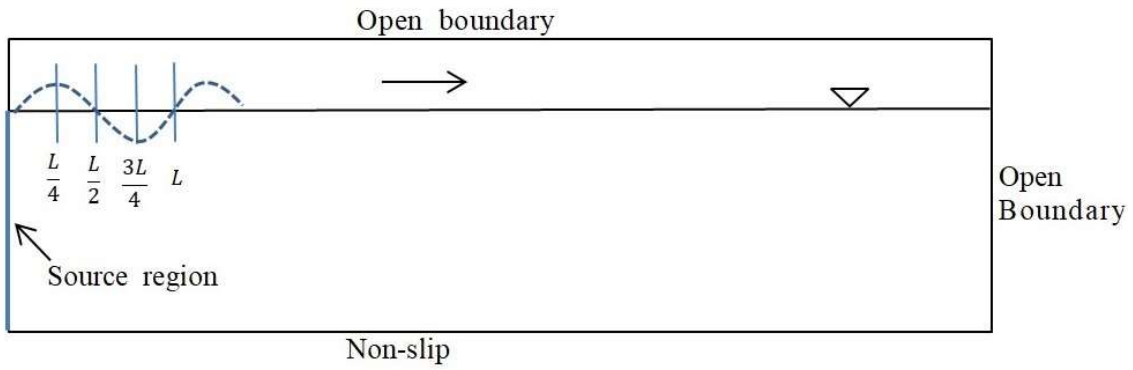

Figure 5.1 Schematic diagram for wave generation with source function.

For nonlinear wave with a short to intermediate wavelength, when the ratio of wave height to water depth H/h exceeds 0.05, Stokes wave theory can be applied (Lin et al., 1999). Fig 5.2 shows the second-order stokes wave propagation at x= 0.25 λ, 0.5 λ, 0.75 λ, 1.0 λ. The closer to the source area, the shorter time it takes for the leading wave to reach this location, but no matter where it is, the wave surface will eventually reach a steady state and agrees with the analytical solution.

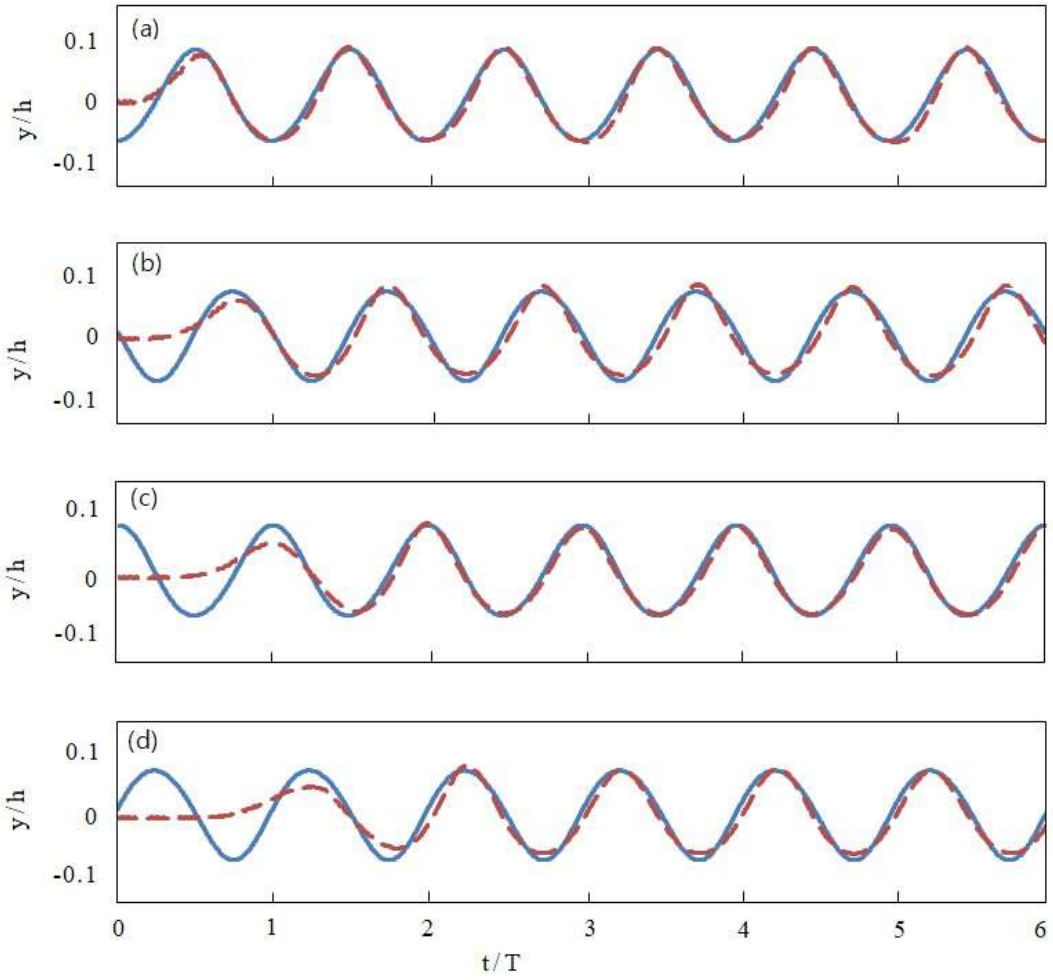

Figure 5.2 Comparisons between Numerical Results (– – -) and Analytical Solutions (——) of Linear Wave Propagation on Constant Water Depth at: (a) x = 0.25 λ ; (b) x = 0.50 λ ; (c) x = 0.75 λ ; (d) x = 1.0 λ.

Fig 5.3 shows the second-order stokes waves propagation at 2T, 3T, 4T, 5T, 6T. The comparison between the wave height and the analytical solution reveals that the numerical simulation results have higher accuracy. In terms of wave phase, the numerical data is better matched to the theoretical data near the source region. The large difference in the second-order Stokes wave test is mainly caused by the low-order approximation in the wave theory.

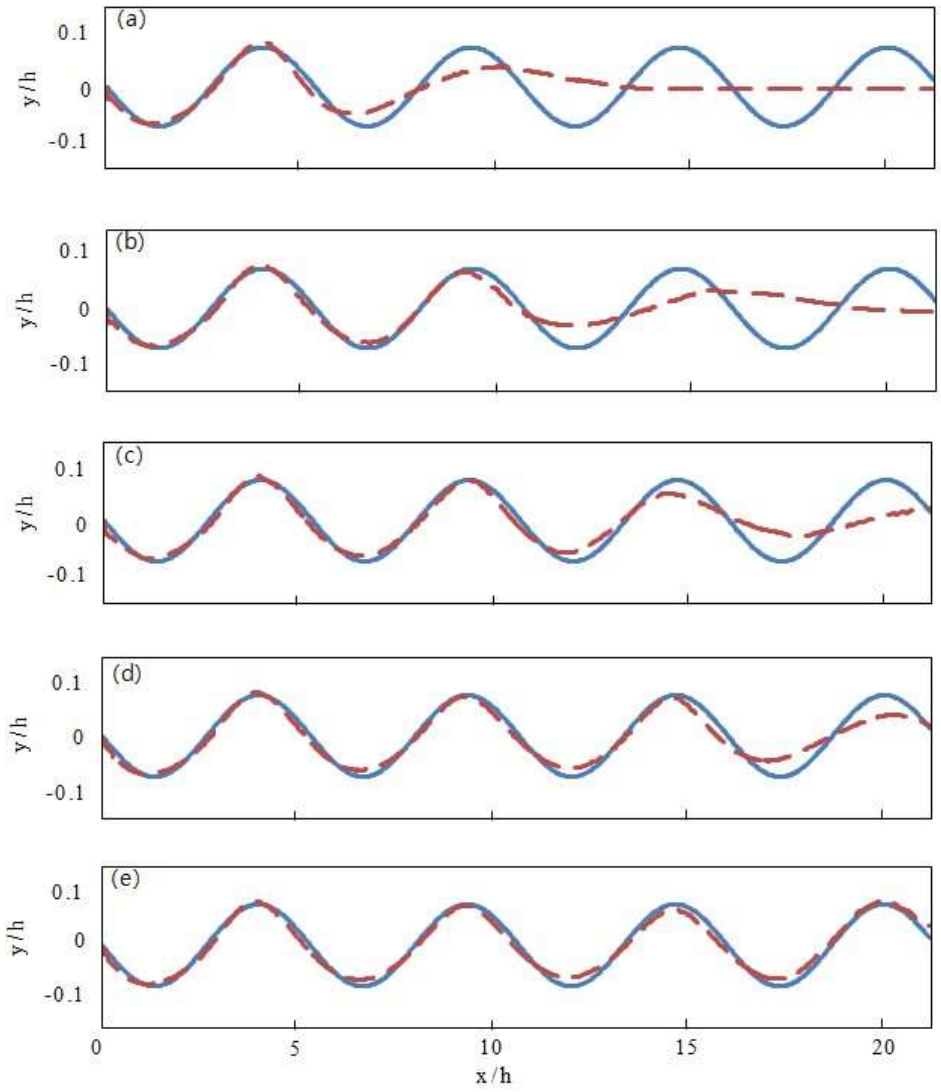

Figure 5.3 Comparisons between Numerical Results (– – ·) and Analytical Solutions (———) of Linear Wave Propagation on Constant Water Depth at: (a) t/T = 2 ; (b) t/T = 3 ; (c) t/T = 4 ; (d) t/T=5 ; (e) t/T = 6.

Therefore, in this chapter, we can conclude that the numerical wave generated by the single-relaxation-time LBGK model and VOF, and the internal mass source method agree well with the theoretical wave.

Chapter 6

The fluid flow past circular and rectangular cylinder under a second stokes wave

When the fluid passes through the submerged body, due to the water depth get shallower on the submerged body, the wave nonlinearity increases, which will cause most of the locked waves to be converted into free wave forms. The change of the wave field will affect the submerged body itself and the post-submerged engineering structure have a great impact. For cylindrical wave breaker, horizontal circular cylinders are the more commonly used. Therefore, in order to find a horizontal cylinder that effectively reduces the wave height, the wave height changes of the fluid passing through a circular cylinder and a rectangular cylinder are simulated in this chapter, and their results are compared and analyzed.

6.1 Case of single circular cylinder and single rectangular cylinder

6.1.1 Computational set-up

For the simulation of flow past a circular cylinder, a computation size of domain is the same as chapter 5. A geometry sketch is shown in Figure 6.1. The diameter of the circular cylinder is set as D = 0.002m which is equal to the sides of a rectangular cylinder. The distance from the mass source generation to the cylinder center is set as l = 0.0614m. And the distance from the bottom of the domain to the cylinder center is set as h0 = 0.0073m. In Fig 6.2, we can see that the rectangular cylinder is in the same position as the circular cylinder when it is in the computational domain, and the width of the rectangular cylinder is equal to the diameter of the circular cylinder.

At inlet boundary, we use mass source method to calculate the LBM distribution function. On bottom walls, we use non-slip bounce-back boundary condition. On upper walls and outlet boundary, we used open boundary condition. On the surface of the cylinder, we use boundary condition proposed by Bouzidi et al. [20].

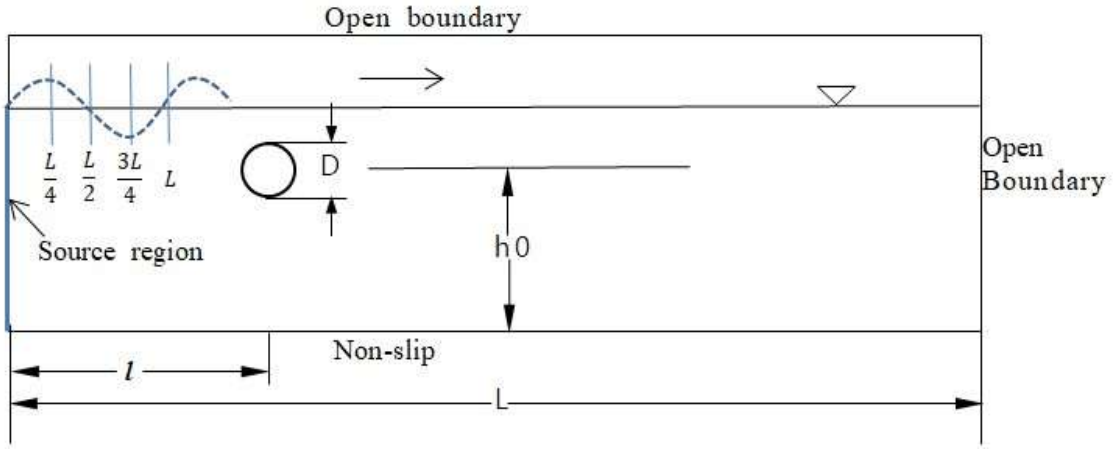

Figure 6.1 Schematic diagram for fluid flow around circular cylinder under a second stokes wave.

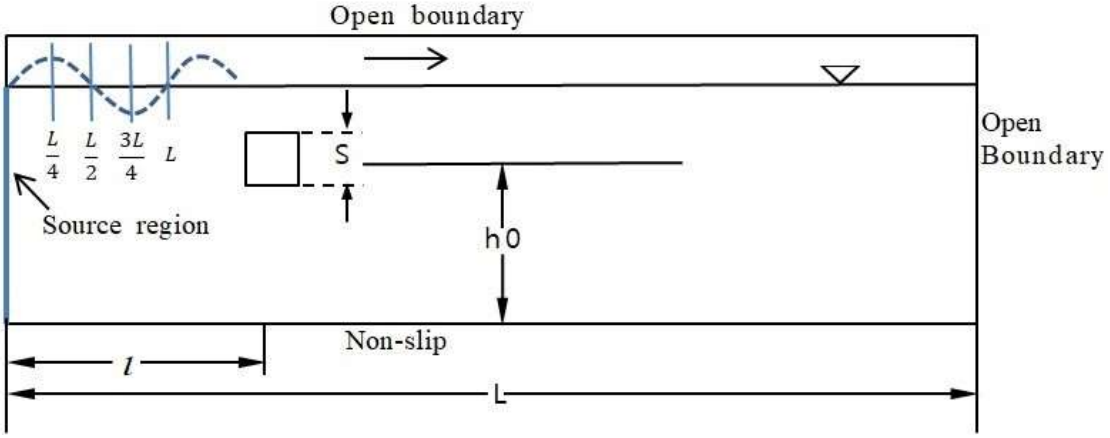

Figure 6.2 Schematic diagram for fluid flow around rectangular cylinder under a second stokes wave.

6.1.2 Numerical experiments

Through the simulation of the above model, we compare the wave height changes before and after the structure. As shown in Fig 6.3, we can see that the wave surface flowing through the structure, the wave height has different degrees of decline, and the wave surface becomes more moderate. For circular cylinder, wave height decreases 8.56 %. For the rectangular cylinder, wave height decreases 10.23 %. Therefore, rectangular cylinder have better wave-cancelling effects.

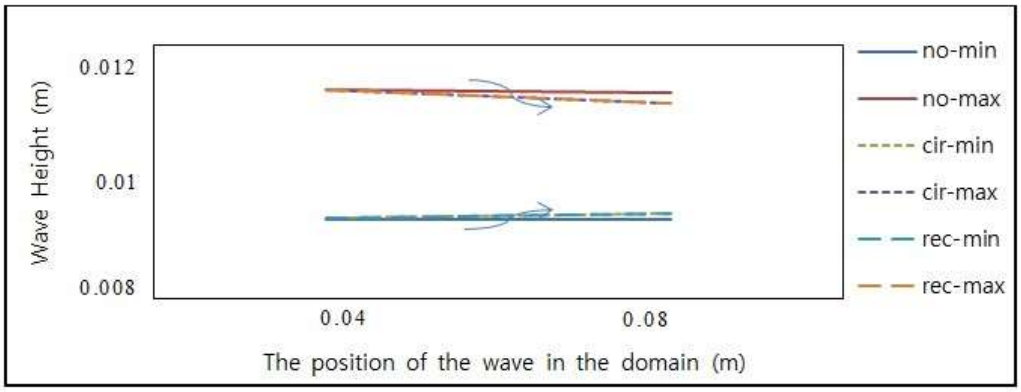

Figure 6.3 The wave height of a circular cylinder and a rectangular cylinder changes with position of wave.

As shown in Fig 6.4 and Fig 6.5, in x direction, we can see that the range of the small velocity around rectangular cylinder is bigger than circular cylinder, but the fluid velocity is faster above the rectangular cylinder. This is due to the different separation points when the fluid passes through the two cylinders. Similarly, in y direction, although the two velocity contours are not much different, we can still see that the velocity around the rectangular cylinder is greater than that of the circular cylinder. In Fig 6.6, we can also clearly see that the vorticity at the four corners of the rectangular cylinder is significantly more than that of the circular cylinder. Therefore, we can conclude that the wave height of the fluid decreases faster and reaches a steady state when it passes through a rectangular cylinder.

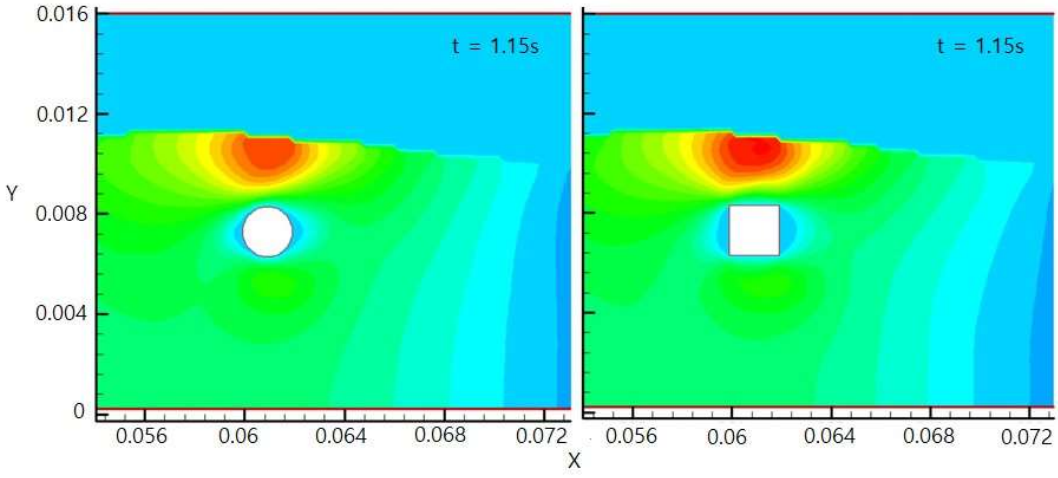

Figure 6.4 Velocity contour of fluid flow past a circular cylinder and a rectangular cylinder in x direction (u).

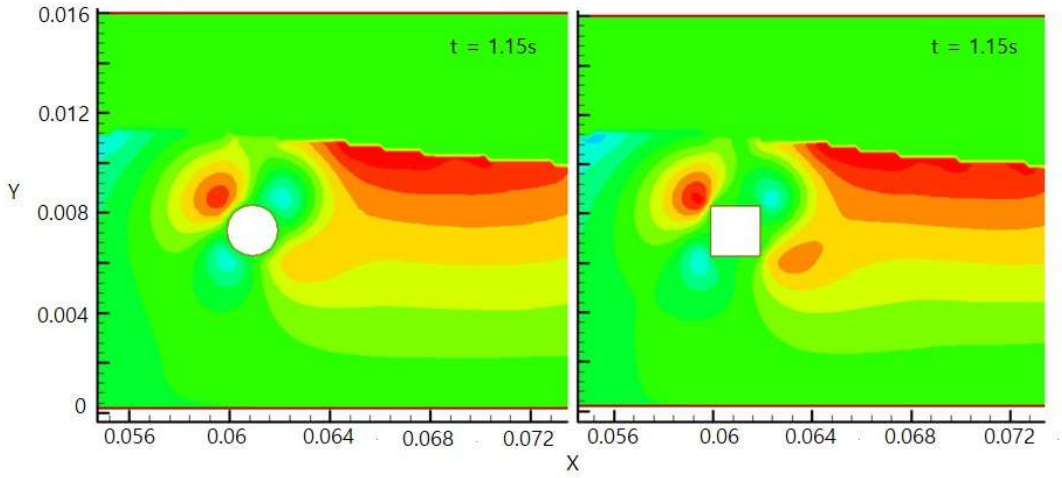

Figure 6.5 Velocity contour of fluid flow past a circular cylinder and a rectangular cylinder in y direction (v).

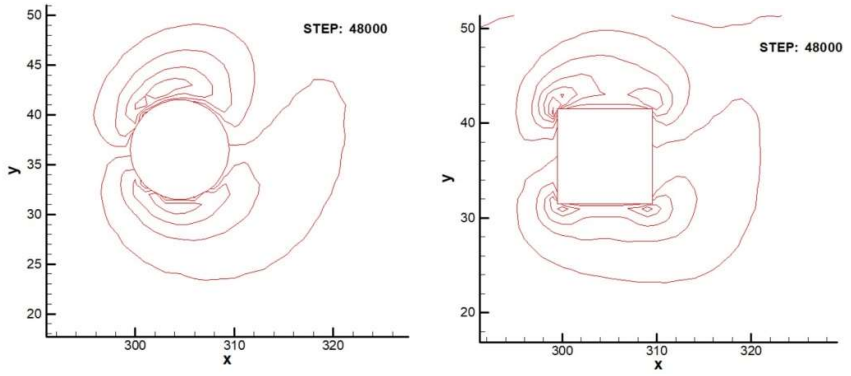

Figure 6.6 Vorticity contour of fluid flow past a circular cylinder and a rectangular cylinder.

6.2 In case of 2 by 2

From the previous section, we learned that rectangular sections have better wave cancellation effects than circular sections. In order to more clearly compare the reduction of wave height under two different cross sections, in this section, we perform numerical simulation on the cylinder group.

6.2.1 Computational set-up

In case of 2 x 2, the distance between the center points of the two structures is 1.5 times the diameter of circular cylinder, other parameters and boundary conditions remain unchanged(see figure 6.7 and figure 6.8).

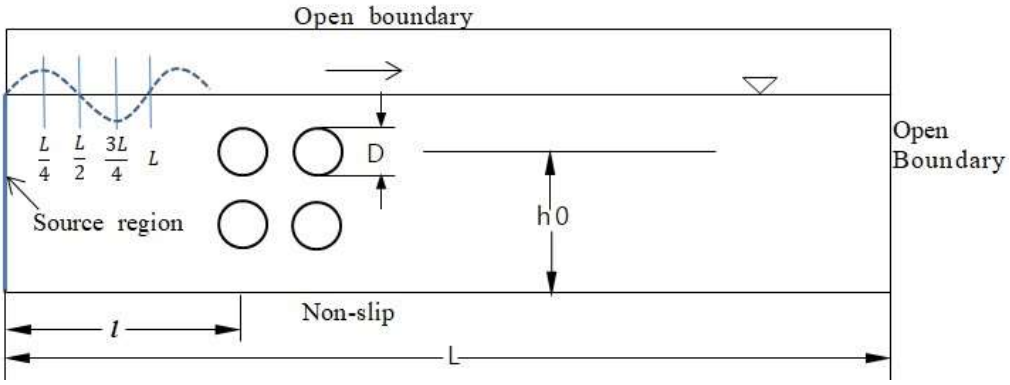

Figure 6.7 Schematic diagram for fluid flow around multi-circular cylinders under a second stokes wave.

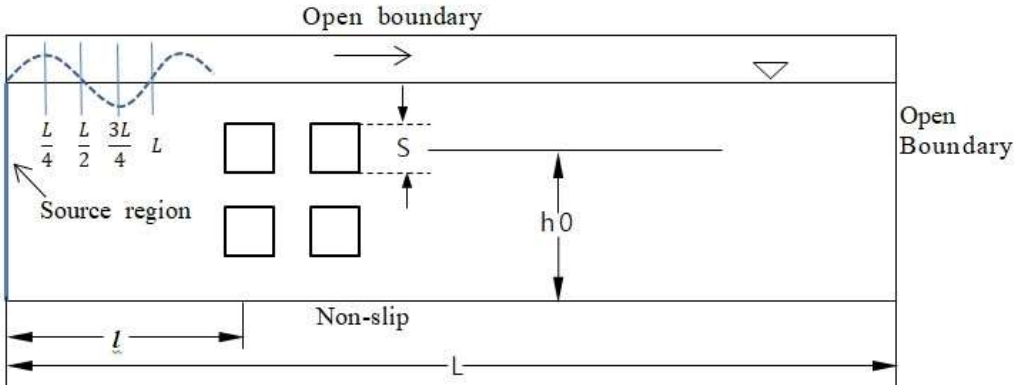

Figure 6.8 Schematic diagram for fluid flow around multi-rectangular cylinders under a second stokes wave.

6.2.2 Numerical experiments

The wave height change of a fluid as it passes through multiple structures is given by the figure below (Figure 6.9). For circular cylinder, wave height decreases 18.89 % . For the rectangular cylinder, wave height decreases 21.12 % . The clipping effect of multiple structures is significantly better than that of a single structure.

Changes in wave height before and after the structure are shown in Fig 6.9, Compared with the initial flow field, the wave height before and after the fluid passes through the rectangular cylinder shows a trend of increasing first and then decreasing. The wave height near the mass source is consistent with the wave height in the initial fluid domain. However, the wave height increases significantly near multi-structures. This shows that the fluid is

affected by multi-structures and does not reach the mass source. Therefore, the placement of multi-structures is reasonable. Fig 6.10 shows the vorticity contour of the column group.

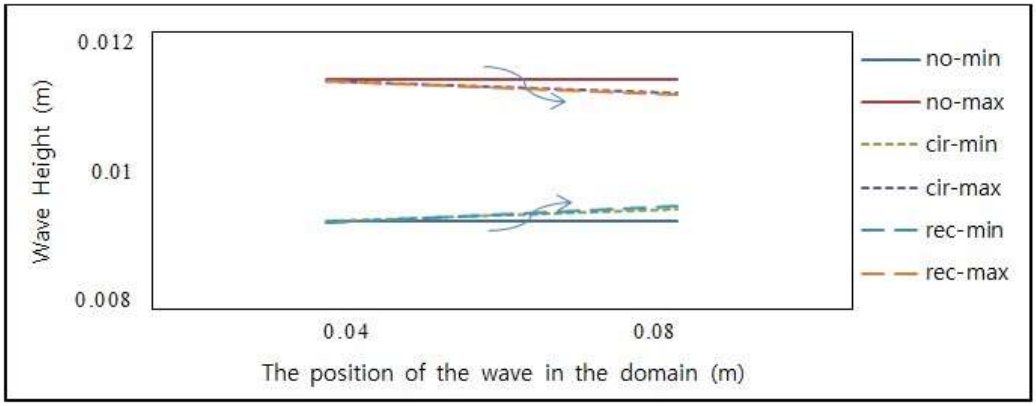

Figure 6.9 The wave height of a circular cylinder and a rectangular cylinder changes with position of wave.

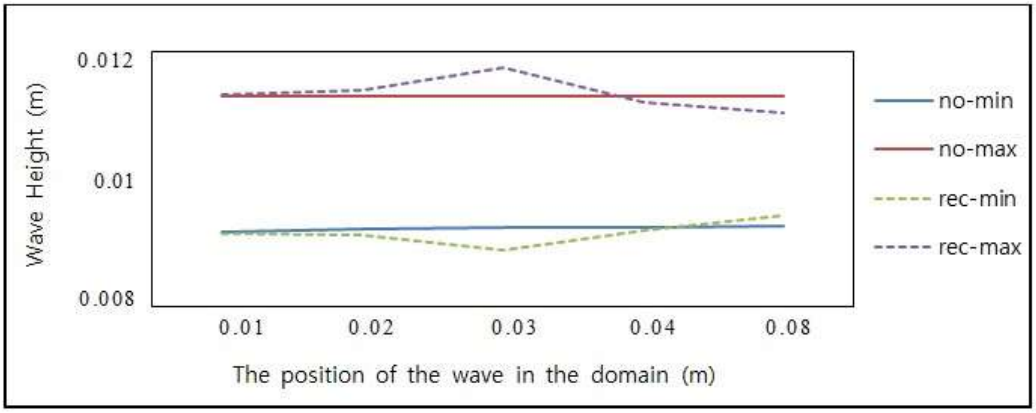

Figure 6.10 The wave height of a rectangular cylinder changes with position of wave.

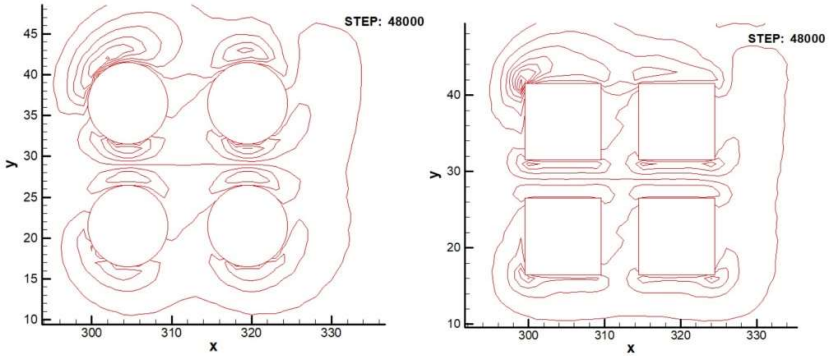

Figure 6.11 Vorticity contour of fluid flow past multi-circular cylinders and multi-rectangular cylinders.

Chapter 7

Wave Breakers

With the development of the marine gas and oil extraction industry, the waves generated by the huge coastline will cause great damage to ships and offshore platforms; and with the development of the fishing industry, in order to protect fishing vessels and the development of the offshore economy, The study of the attenuation of the waves and the structure of the wave protection facilities has attracted the attention of scholars around the world. From the previous chapter, we can see that multiple rectangular cylinders can achieve better wave cancellation effects. Therefore, in this chapter we simulate the small-scale multi-structure wave-eliminating characteristics, and compare the wave height change with the initial value.

7.1 Fluid flow past multi-structures

7.1.1 Computational set-up

Based on the previous simulation data, the sides of the rectangular and the distance between the structures are reduced. The side length of the rectangular is 0.0016 m, the distance between the structures is 0.0004 m. Other parameters and boundary conditions remain unchanged. Simulates three different forms of multi-structures, 2 by 2, 3 by 3, 4 by 4.

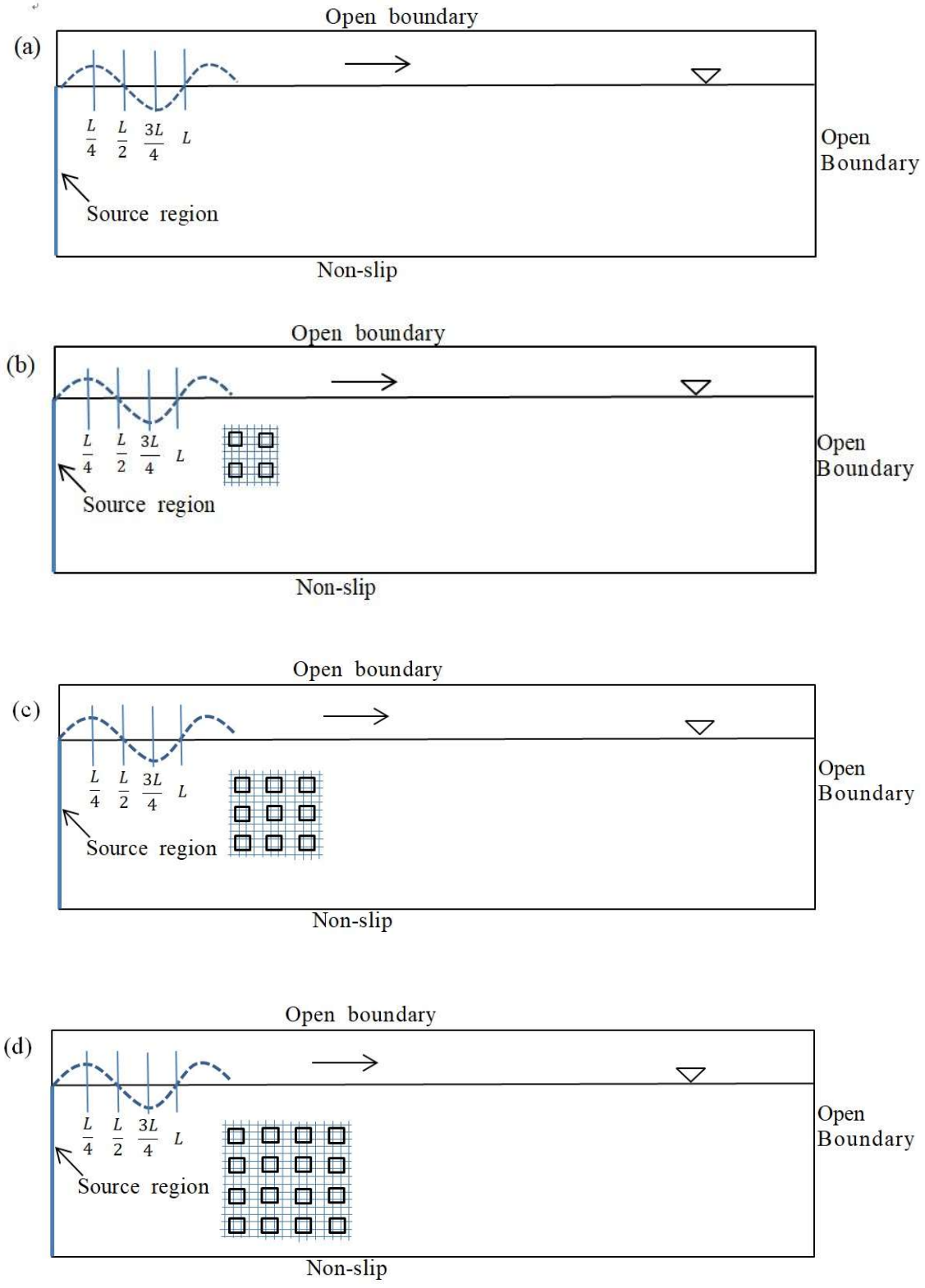

Figure 7.1 Schematic diagram for fluid flow though several different multi-structures, (a) original fluid domain, (b) 2 x 2, (c) 3 x 3, (d) 4 x 4.

7.1.2 Case Study

In order to find a stable square cylinder structure with the best wave-eliminating effect, first reduce the size of the rectangle and set the same gap here, so the influence of the gap size on the waves is not considered. The free liquid level values before and after the porous structure were obtained by simulating the three different porous structure models described in Section 7.1 and compared to the wave height of the initial flow field. The porous structure in (d) has the most pronounced wave-eliminating effect, the amplitude of the wave height is reduced by 33.63%, and the second is effective of the structure of (c), which lowers 21.55 %, Compared with the initial flow field, (b) has the least effect of wave-eliminating effect, which is reduced by 15.82 %. Therefore, we can see that the wave-eliminating effect increases as the porous structure increases. The elimination of the characteristics of the free surface wave of the porous structure depends not only on its porosity but also on the pore structure having a smaller pore size. The structural dimensions used in this article are too small. Considering practical engineering applications, porous structures that are too small in size may not achieve the desired wave-eliminating effect. Therefore, the mesh size should be appropriately increased to achieve better wave-eliminating efficiency. Even so, through the research and analysis, the use of a square porous structure can also have a good wave-eliminating effect, which verifies its feasibility.

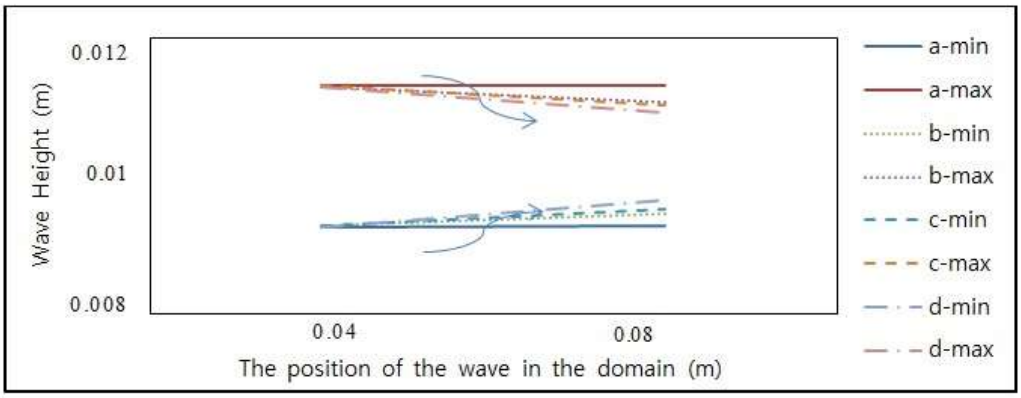

Figure 7.2 Wave height at different locations as the wave flows through different types of multi-structures.

7.2 Fluid flow past plate structure

This section expands the simulation of flat plate wave cancellation. The slab can be used as a new type of breakwater. This breakwater can be arranged in front of large marine structures to prevent huge waves from directly acting on the structure. It can also be built near the coastline erosion area or marine culture area to reduce the wave force directly Function to reduce the ship's energy in waves and protect coastal geology and geomorphology. However, there are many types of boards, and there are many factors that affect the wave-cutting effect. How to effectively wave-cut and which type of plate can achieve the maximum wave-cutting effect are the main considerations. Wang Ke et al. Studied the wave elimination characteristics and wave elimination mechanism of horizontal plate breakwaters near free surface in 2016[33]. In this chapter, we mainly study the effect of board length on wave elimination. The position where the board is immersed in water is fixed and the width of the board is determined. Therefore, we will not consider these factors for the time being.

7.2.1 Numerical experiments

Based on the fluid domain conditions described in Chapter 5, we place the board at h0 = 0.0079 m, h0 is the distance from the center of the plate to the bottom. Set three different board widths 1/6λ, 1/3λ and 1/2λ, respectively. The distance from the plate to the entrance is about one wavelength.

(a)

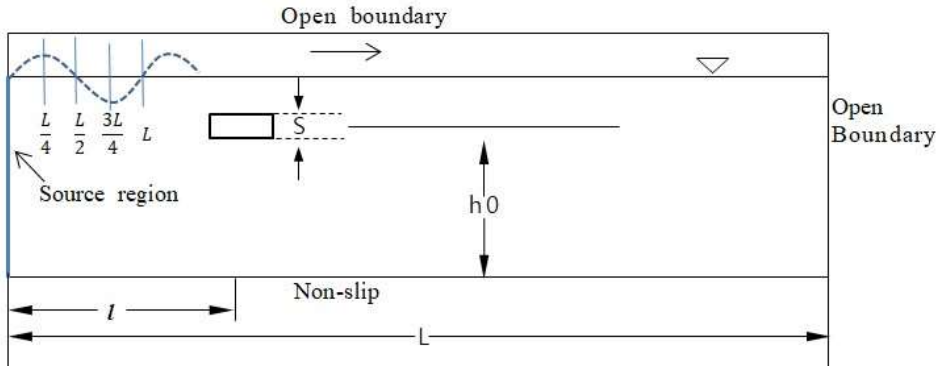

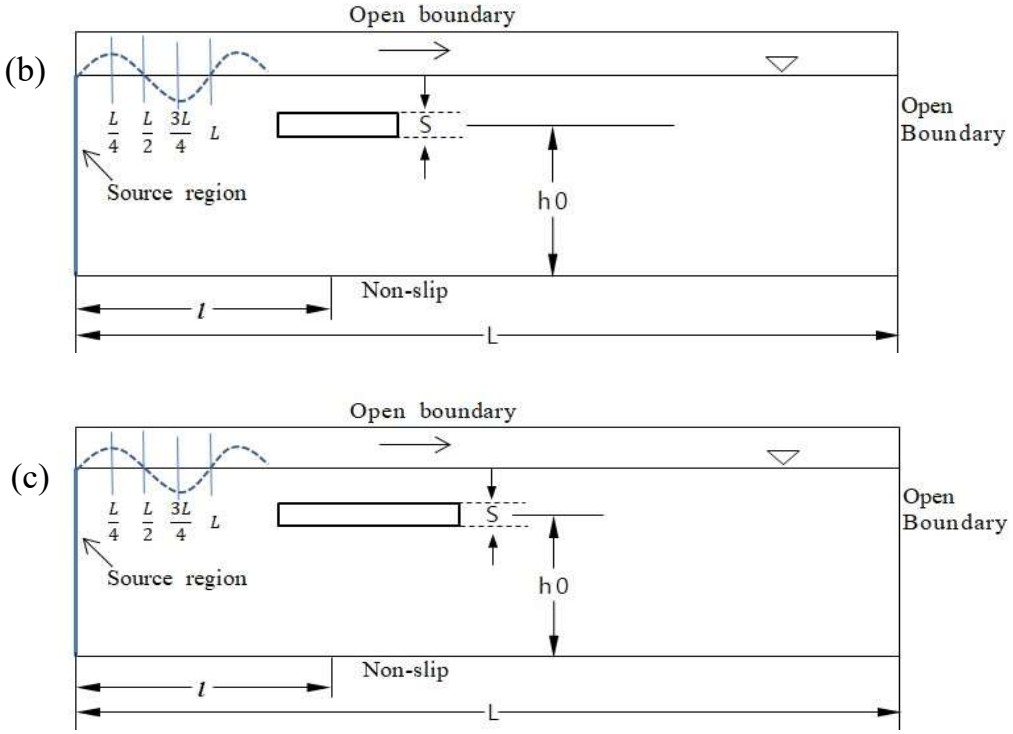

Figure 7.3 Schematic diagram fluid flow through three different plates with (a) 1/6λ, (b) 1/3λ (c) 1/2λ.

By simulating these three horizontal plates of different lengths, when the length is s1, the wave height is reduced. When the length of plate equal 1/6λ, the wave height decreases 47.46 %. When the length of plate equal 1/3λ, the wave height decreases 75.55%. When the length of plate equal 1/2λ, the wave height decreases 71.79%. Among them, when the plate length is 1/3λ the highest degree of wave height reduction, this is consistent with the data of Wang Ke et al [33]. So we only need 1/3λ -length boards to get the required wave. Figure 7.4shows the density distribution of plate at different times, we can see that when the wave enters the shallow water area submerged on the horizontal plate, the wavelength will become shorter and the wave surface will rise. The transmitted wave behind the plate will produce a large phase difference, and there will be strong non-linearity in the water area short from the plate effect. The front of the plate is subjected to wave force, and the phenomenon of backflow occurs behind the plate. This backflow phenomenon and the disturbance of the water body around the plate are the main reasons for the deformation of the free liquid surface. At this time, the wave is decomposed into a series of high-frequency short waves, and this high-frequency short wave quickly dissipates energy around the plate, which greatly attenuates the transmitted wave amplitude. Figure 7.5 shows at time t = 1.15s, velocity

contour with plate length equal 1/3λ. The speed is mainly concentrated on the force side and above the board.

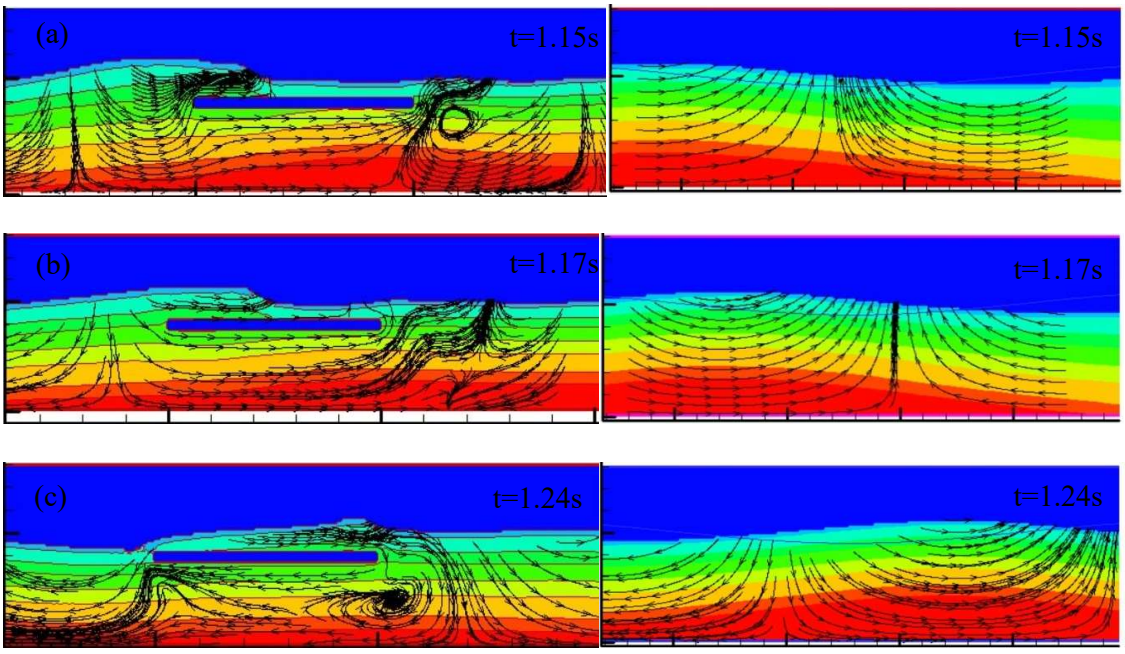

Figure 7.4 Density contours of plate compare with Initial flow field at different times: (a) t = 1.15s, (b) t = 1.17s, (c) t = 1.24s.

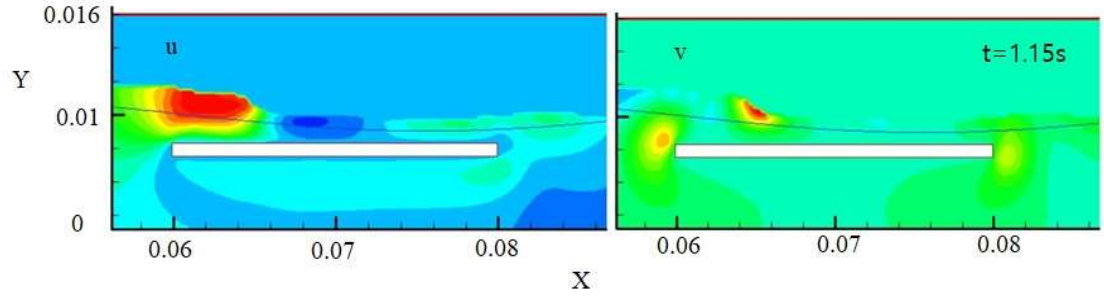

Figure 7.5 Velocity contours of plate at u and v direction at t = 1.15s.

Chapter8

Conclusion

The lattice Boltzmann method (LBM) is widely used for its simple programming which mainly consists of the term of collision and streaming. Comparing with the Navier-Stokes solver, the collision term and streaming term can be interpreted by viscous and convection behavior, respectively. This thesis is applied LBM simulation to be implemented to wave height reduction effect under a progressive wave. Through some set of multi-structures media are setup under the wave, we tried to find out the reduction effect in numerically.

In order to simulate the wave height reduction effect, some basic programming is implemented in simulation code. First, a wave maker is implemented by the mass source method which is added force term in LBM govern equation. The force is given through a line for inlet boundary condition based on a linear monochromatic wave. Some set of porous media which is consisted by small rectangles are fixed under a wave. Three cases are simulated by 2 by 2, 3 by 3 and 4 by 4. For the computational stability, the multi-relaxation time is adapted.

For the simulation, some validations have done. In case of free surface simulation, a second order Stokes wave is simulated and compared with the analytical solution. The treatment is based on VOF (volume of fluid) type free surface simulation.. It should be noted that the grid system used here is uniform and the contours of the waves may be jagged in certain parts. To make the wave surface profile smoother, a multi-grid system should be used near the free surface area.

By simulating single and multiple circular and rectangular cylinders, it can be seen that the rectangular cylinder has better wave elimination performance. By inserting a multi-structures into the fluid domain and simulating the arrangement of the three different forms, the results show that the addition of each form of porous structure can reduce the wave height and effectively mitigate the reflection problem caused by vorticities generated from the structures. Regardless of the effect of porosity, a small-sized porous structure can better achieve the effect of wave-eliminating. Thus, under the same porosity, the arrangement and width of the porous structure are the key factors that control the wave elimination effect. For

a rectangular cylinder, the case of 4×4 has the best wave cancellation performance and can reduce the wave height of 33.63%.

For the plate type wave-reducing structure, the length of the plate directly determines the quality of wave-cutting performance. Therefore, choose the case of L = 1/3λ, you can get the ideal wave-cutting effect, and the wave-cutting effect is as high as 75.55%.

Through this simulation which a suitable type of porous structure can achieve the wave-eliminating effect, LBM is a useful tool for a costal engineering application.

References

[1] Chen S, Chen, H D, Martinez D, et al. “Lattice Boltzmann model for simulation of magneto-Hydrodynamics”. Physical Review Letters, 1991, 67(27): 3776-3779.

[2] He, X. and Luo, L. S., 1997, “Lattice Boltzmann Model for the Incompressible Navier-Stokes Equation”, Journal of Statistical Physics, 88, pp. 927-944.

[3] Pan C, Luo L, Miller C T. 2006, “An evaluation of Lattice Boltzmann schemes for porous medium flow simulation”. Computers & Fluids, 35: 898-909.

[4] Yu H, Girimaji S S. 2005, “Near-field turbulent simulations of rectangular jets using lattice Boltzmann method”. Physics of Fluids, 17: 125106.

[5] Yu H, Girimaji S S. 2006, “Lattice Boltzmann equation simulation of rectangular jet (AR=1.5) instability and axis-switching. Physica A, 362:151-157.

[6] Yu H, Luo L, Girimaji S S. 2006, “LES of turbulent square jet flow using an MRT lattice Boltzmann model”. Computers & Fluids, 35:957-965.

[7] Liu Y, So R M C, Cui Z X. 2006, “ Bluff body flow simulation using lattice Boltzmann equation with multiple relaxation time. Computers & Fluids, 35:951-956.

[8] Mccracken M E, Abraham J. 2005, “Multiple-relaxation-time lattice-Boltzmann model for multiphase flow”. Physical Review E, 71: 036701.

[9] S. Hou, J. Sterling, S. Chen and G. D. Doolen, 1996, “A lattice Boltzmann sub-grid m odel for high Reynolds number flows”, in: Lawniczak AT, Kapral R, editors. Pattern f ormation and lattice gas automata. Fields Inst Commu, vol. 6, p. 151–66.

[10] Manfred Krafczyk , Jonas Tolke, 2003, “Large Eddy simulations with a Multiple-Rela xation-Time LBE model”, International Journal of Modern Physics B, Vol. 17, Nos. 1 & 2 33-39.

[11] Myata. H, Kajitani. H, Zhu. M. 1987, “Numerical Study of Some Wave-breaking Problems by a Finite Difference Method [J]”.The Japan Society of Naval Architects and Ocean Engineers. (207): 12-22.

[12] Brorsen. M. Larsen. J. 1987, “Source Generation of nonlinear gravity waves with boundary integral equation method”. Coastal Engineering. (11): 93-113p.

[13] Lin, P, Liu, PLF, 1999, “Internal wave-maker for Navier-stokes equations models”, Port, Coastal and Ocean Engineering, 125(4), 207-217.

[14] Wang.K, Yu.Y, Yang.L, Hou. Guoxiang, 2017, “Lattice Boltzmann based internal wave-maker”, Int. Ocean .and. Polar. Eng. Conf.

[15] Shan, G. 2003, “Establishment and application of two-dimensional numerical wave trough mode and study of wave current”. Ocean University of China.

[16] Troch. P. and Rouck. J. D. 1998, Development of two-dimensional numerical wave flume for wave interaction with rubble mound breakwaters. [C]. Proceedings of 26th Conference on Coastal Engineering. 1638-1649.

[17] Bhatnagar, P. L., Gross, E. P. & Krook, M., 1954, “A model for collision processes in gases. i. small amplitude processes in charged and neutral one-component systems”, Physical review,94(3):511.

[18] D. d’Humières, 1992, “Generalized lattice Boltzmann equation. In Rarefield Gas Dynamics: Theory and Simulations, Progress in Astronautics and Aeronautics”, B.D. Shizgal, D.P. Weaver (Eds.), vol. 159, p. 450.

[19] Q. Zou and X. He, 1997, “On pressure and velocity boundary conditions for the lattice Boltzmann BGK model”, Phys. Fluids, 9, 1592-1598.

[20] M’hamed Bouzidi, Mouaouia Firdaouss, and Pierre Lallemand, 2001, “Momentum transfer of a Boltzmann-lattice fluid with boundaries”, Physics of Fluids, 13, 3452.

[21] Thùrey, N, Rùde, U, Körner, C, “Interactive free surface fluids with the lattice Boltzmann method”, Technical Report 05-4. University of Erlangen-Nuremberg, Germany.

[22] Thùrey, N, 2007, “Physically based animated of free surface flows with the lattice Boltzmann method”, Ph.D. Thesis, University of Erlangen-Nuremberg, Germany.

[23] Z. Guo, C. Zheng and B. Shi., 2002, “An extrapolation method for boundary conditions in lattice Boltzmann method”. Phys. Fluids, 14, 2007-2010.

[24] Finck M, Hanel D, Wlokas, 2007, “Simulation of nasal flow by lattice Boltzmann methods”, Comput. Bio. Med. 37:739-749.

[25] R. W. Mei, D. Z. Yu, W. Shyy, and L. S. Luo, 2002,”Phys. Rev. E 65, 041203.

[26] H. B. Li, X. Y. Lu, H. P. Fang, and Y. H. Qian., 2004, Phys. Rev. E 70, 026701.

[27] Martin B. Schlaffer, 2013, “Non-reflecting Boundary Conditions for the Lattice Boltzmann Method”. Technische Universität München, Lehrstuhl Für Computation in Engineering.

[28] Chen Tongqing, Zhang Qinghe, Cheng Liang, 2010, “Performance Investigation of 2D Lattice Boltzmann Simulation of Forces on a Circular Cylinder”, Transactions of Tianjin University Vol.16 No.6.

[29] Beaudan P, Moin P, 1994, “Numerical Experiments on the Flow Past a Circular Cylinder at Sub-critical Reynolds Number”, Report No. TF-62[R]. Department of Mechanical Engineering, Stanford University.

[30] Kravchenko A G, Moin P, 2000, “Numerical studies of flow over a circular cylinder at Re=3900”, Physics of Fluids, 12(2): 403-417.

[31] Guo, ZL, Zheng, CG, Shi, BC, 2002, “Discrete lattice effects on the forcing term in the lattice Boltzmann method”, Physical Review E, 65(4), 046308.

[32] Wiegel, R.L, 1960, “A presentation of cnoidal wave theory for practical application.” J. Fluid Mech., Cambridge, U.K., 7, 273-286.

[33] Wang K, Xu W, Zhang ZQ, 2010, “Study on Wave Suppression Characteristics and Mechanism of Horizontal Plate Breakwater Near Free Surface”, Vol. 14 No. 4.